

LASER INTERFEROMETER GRAVITATIONAL WAVE OBSERVATORY
- LIGO -

CALIFORNIA INSTITUTE OF TECHNOLOGY
MASSACHUSETTS INSTITUTE OF TECHNOLOGY

| | | | |
|-------------------------------------------------------------------------------------------------|-------------------|--------------|-------------|
| Technical Note | LIGO-T980044-07 | -E | 99.07.29 |
| <i>Document</i> | <i>Doc Number</i> | <i>Group</i> | <i>Date</i> |
| Determination of Global and Local Coordinate Axes for the LIGO Sites <i>Title</i> | | | |
| William Althouse Larry Jones Albert Lazzarini <i>Author[s]</i> | | | |

This is an internal working note of
the LIGO Project

California Institute of Technology
LIGO Project - MS 18-33
Pasadena CA 91125
Phone +1.626.395.2966
Fax +1.626.304.9834
E-mail: info@ligo.caltech.edu

Massachusetts Institute of Technology
LIGO Project - MS 20B-145
Cambridge, MA 01239
Phone +1.617.253.4824
Fax +1.617.253.7014
E-mail: info@ligo.mit.edu

WWW: <http://www.ligo.caltech.edu>

Table of Contents

| | | |
|-----|-------------------------------------------------------------------------------|----|
| 1 | Purpose..... | 4 |
| 2 | Hanford Survey Data | 5 |
| 2.1 | Fit to the Survey Data | 9 |
| 2.2 | Error propagators in the fits | 13 |
| 2.3 | Hanford Local Coordinate Systems in each station..... | 17 |
| 3 | Livingston Survey Data | 18 |
| 3.1 | Fit to the Survey Data | 23 |
| 3.2 | Error propagators in the fits | 29 |
| 3.3 | Livingston Local Coordinate Systems in each station..... | 35 |
| 3.4 | Positions of LIGO Primary GPS Monuments in the Global Coordinate System | 36 |
| 4 | Graphical representations of the interferometer planes for each site..... | 38 |

List of Figures

| | | |
|-----------|-------------------------------------------------------------------------------------------------------------------------------------------------------------------------------------------------------------------|----|
| Figure 1: | Geodetic and Earth-Fixed Coordinates..... | 9 |
| Figure 2: | Scatter plots of fit residuals in plane normal to global axis for Hanford, WA. | 12 |
| Figure 3: | Dependence of residuals on distance along the arms, Hanford, WA..... | 12 |
| Figure 4: | Pitch, yaw, and roll axes for the orientation error analysis..... | 13 |
| Figure 5: | Scatter plots of fit residuals in plane normal to global axis for Livingston, LA..... | 28 |
| Figure 6: | Dependence of residuals on distance along the arms for Livingston, LA. | 28 |
| Figure 7: | Layout of the CB&I control points and primary GPS monument array at Livingston. Dots (colored) denote the CB&I control points for alignment of the beam tubes; plus signs denote the primary GPS monuments. | 37 |
| Figure 8: | Representation of the interferometer plane inclinations at the two LIGO sites..... | 39 |

List of Tables

| | | |
|-----------|----------------------------------------------------------------------------------------------------------------------------------------------------|----|
| Table 1: | Relevant, Previously Released LIGO Documents | 4 |
| Table 2: | Design values of the global coordinate positions of BT/VE interface markers..... | 5 |
| Table 3: | Cardinal Marker Survey Data for Hanford | 6 |
| Table 4: | Parameters resulting from best fit to the survey data for Hanford, WA..... | 10 |
| Table 5: | Global coordinate positions of as-built BT/VE interface markers..... | 11 |
| Table 6: | Sensitivity matrix for the XG coordinate for BTVE markers..... | 14 |
| Table 7: | Sensitivity matrix for the YG coordinate for BTVE markers..... | 15 |
| Table 8: | Sensitivity matrix for the ZG coordinate for BTVE markers | 16 |
| Table 9: | Uncertainties in fitted parameters. Changing the best fit values by these amounts re- sult in a doubling of the RMS residual fitting error..... | 17 |
| Table 10: | Hanford Vertex Global-Local System Direction Cosines | 17 |
| Table 11: | Hanford X End Station (d= 4000m) Global-Local System Direction Cosines..... | 17 |
| Table 12: | Hanford Y End Station (d= 4000m) Global-Local System Direction Cosines..... | 18 |
| Table 13: | Hanford X Mid-Station (d = 2000m) Global-Local System Direction Cosines | 18 |
| Table 14: | Hanford Y Mid-Station (d = 2000m) Global-Local System Direction Cosines | 18 |
| Table 15: | Design values of the global coordinate positions of BT/VE interface markers..... | 19 |
| Table 16: | Cardinal Marker Survey Data for Livingston | 20 |
| Table 17: | Control Point CB&I Survey Data | 22 |

| | | |
|-----------|-----------------------------------------------------------------------------------------------------------------------------------------------|----|
| Table 18: | Parameters resulting from best fit to the survey data for Livingston, LA | 24 |
| Table 19: | Global coordinate positions of as-built BT/VE interface markers..... | 25 |
| Table 20: | Global coordinate positions of CB&I control points, meters | 26 |
| Table 21: | Sensitivity matrix for the XG coordinate for control points | 29 |
| Table 22: | Sensitivity matrix for the YG coordinate for control points | 31 |
| Table 23: | Sensitivity matrix for the ZG coordinate for control points | 33 |
| Table 24: | Uncertainties in fitted parameters. Changing the best fit values by these amounts result in a doubling of the RMS residual fitting error..... | 35 |
| Table 25: | Livingston Vertex Global-Local System Direction Cosines | 35 |
| Table 26: | Livingston X End Station (d= 4000m) Global-Local System Direction Cosines.. | 35 |
| Table 27: | Livingston Y End Station (d= 4000m) Global-Local System Direction Cosines.. | 36 |
| Table 28: | Report Geodetic Coordinates for the GPS primary monuments at Livingston | 36 |
| Table 29: | Position of the GPS primary monuments in the site global coordinate system..... | 38 |

1 PURPOSE

This document uses survey data taken during the course of fabricating the beam tubes at the LIGO Observatories to determine the as-built orientation and origin for the LIGO Site Coordinate Axes.

Table 1 lists previously issued documents that contain relevant information. The present document supersedes previously released determinations of the coordinate axes because more information is now known about the as-built beam tube and marker geometry. Some earlier analyses used a spherical earth model. At that time, the rough data that were available could be adequately described; later, higher precision GPS data dictated switching to the accepted WGS-84 ellipsoidal model of the earth for refined analyses.

Table 1: Relevant, Previously Released LIGO Documents

| <i>LIGO Document umber</i> | <i>Title</i> | <i>Description</i> |
|--------------------------------|--------------------------------------------------------------------------------------------------------------------------------|---------------------------------------------------------------------------------------------------------------------------------------------------------------------------------------------------------------------------------------------|
| L950128 | LIGO Coordinate System | Gives an operational definition of the site global and local coordinate axes |
| T950004 | Derivation of Global and Local Coordinate Axes for the LIGO Sites | Takes the operational definition and derives the <i>design</i> beam centerline direction cosines, global and local coordinate axes. <u>Uses a spherical model for the earth and Parsons-provided rough grading survey data.</u> |
| T950107 | Orientation of the LIGO Beam Center Lines with respect to foundation slabs | Written for PSI (the VE contractor) to document the angular deviation from local horizontal of the <i>design</i> beam tube centerlines in each of the LIGO stations. <u>Uses data appearing in T950004 (i.e. spherical earth model).</u> |
| T960176 | Determination of the LIGO Global Coordinate Axes for Hanford, WA: final analysis of the LIGO BT/VE interface survey monuments. | Reports the results to a first best-fit determination of the plane defined by the eight cardinal points for the Hanford site. Uses early survey data from RSI and IMTEC. <u>Results are superseded by present, more thorough, document.</u> |
| D950021 | LIGO Arm Layout | Drawing showing BT/VE interface locations |
| C962080 | TDM 014C to CB&I | Provides the height offsets above the marker elevations for establishing the beam tube centerlines at Hanford. |

Table 1: Relevant, Previously Released LIGO Documents

| <i>LIGO Document number</i> | <i>Title</i> | <i>Description</i> |
|-------------------------------------------|-------------------------------------------------------------------------------------------------------------|-----------------------------------------------------------------------------------------------------------------|
| C982209 | Livingston Beam Tube Alignment Data | Provides the CB&I control point data for the arm alignment. |
| C971830-00 C972035-00 C980026-00,-A | LIGO to CB&I Technical Direction Memoranda | Provide survey and design information to CB&I regarding beam line offsets w.r.t BT/VE interface markers |
| C982063-00 | Report on Final Results of the Location of the BT/VE Monuments at the Livingston, Louisiana LIGO Laboratory | Provides the JSB data for the Livingston BT/VE interface markers. |
| SJB Drawing | LIGO Monuments for LIGO Drawn: 5 August 1997 Signed (by Teegarden): 19 September 1997 | Depicts layout of the array of GPS primary monuments: gives latitude, longitude and orthometric height in feet. |

2 HANFORD SURVEY DATA

In the course of laying out the Hanford site, eight cardinal points were surveyed in preparation for fabrication and alignment of the beam tubes. These points defined the interface positions for the beam tube (BT) and vacuum equipment (VE) contracts. These points are identified by suitably inscribed marks on each of eight brass markers, denoted {BT/VE1, ..., BT/VE8} (see D950021 for specifications). The design positions in global coordinates of the interface markers are given in **Table 2**.

Table 2: Design values of the global coordinate positions of BT/VE interface markers

| Marker ID | X_G | Y_G | Z_G |
|-----------|----------|----------|---------------------|
| BT/VE 1 | 0.000 | 46.000 | -1.070 ^a |
| BT/VE 2 | 0.000 | 2007.500 | -1.070 |
| BT/VE 3 | 0.000 | 2027.000 | -1.070 |
| BT/VE 4 | 0.000 | 3988.500 | -1.070 |
| BT/VE 5 | 46.000 | 0.000 | -1.070 |
| BT/VE 6 | 2007.500 | 0.000 | -1.070 |

Table 2: Design values of the global coordinate positions of BT/VE interface markers

| Marker ID | X_G | Y_G | Z_G |
|-----------|----------|-------|--------|
| BT/VE 7 | 2027.000 | 0.000 | -1.070 |
| BT/VE 8 | 3988.500 | 0.000 | -1.070 |

a. The design for the BT centerline was to be 1.070 m above the finished slab.

BT/VE1 - BT/VE4 lie along the Y arm and BT/VE5 - BT/VE8 are similarly arranged along the X arm.

During the course of constructing the beam tubes, the markers were surveyed a number of times by different parties. Sometimes only a subset of the full three-dimensional position of the markers were determined (e.g., height only). In making use of all data, missing information has been substituted using complementary information from other surveys (e.g., height-only data were augmented with $\{\phi, \lambda\}$ data from other measurements). This will tend to artificially tighten the scatter in the those coordinate directions which are affected by the repeated use of the same $\{\phi, \lambda\}$ coordinates; however, this approach allows all height data to be used. This is desirable because height determinations were typically the noisiest and having more measurements serves to improve the level of precision of the dataset as a whole.

Table 3 presents the survey results for the eight BT/VE markers. The markers were placed on the as-built beam tube slabs. Their heights are affected by slight irregularities in the slab finish. After the first survey by IMTEC and RSI, LIGO determined the best estimate (at that time) for the vertical offsets above each of the markers where the beam tube centerline should be located. The last column in the table shows these vertical offsets. The global coordinate axes were determined by fitting to a beam tube centerline going through points at the indicated offsets above the markers. In reporting the marker locations, the offsets were then subtracted from the residuals to the fit in order to refer the monument locations on the slab surfaces.

Table 3: Cardinal Marker Survey Data for Hanford

| <i>Marker ID</i> <i>Source</i> | <i>Latitude[N]</i> | | | <i>Longitude[W]</i> | | | <i>Ellipsoidal height of marker</i> | <i>Design height of beam centerline above marker elevation</i> |
|----------------------------------------------------------|--------------------|----|----------|---------------------|----|----------|-------------------------------------|----------------------------------------------------------------|
| | ° | ' | " | ° | ' | " | <i>m</i> | <i>m</i> |
| <i>BT/VE1</i> | | | | | | | | |
| IMTEC RSI-GroundLoop RSI-GPS CBI-GPS (all same) | 46 | 27 | 17.65230 | -119 | 24 | 29.30959 | 141.4980 | 1.0602 |

Table 3: Cardinal Marker Survey Data for Hanford

| <i>Marker ID Source</i> | <i>Latitude[N]</i> | | | <i>Longitude[W]</i> | | | <i>Ellipsoidal height of marker</i> | <i>Design height of beam centerline above marker elevation</i> |
|-----------------------------|--------------------|----|----------|---------------------|----|----------|---------------------------------------------|----------------------------------------------------------------------------|
| | ° | ' | " | ° | ' | " | <i>m</i> | <i>m</i> |
| <i>BT/VE2</i> | | | | | | | | |
| IMTEC | 46 | 26 | 40.30783 | -119 | 25 | 43.65422 | 141.8340 | 1.0612 |
| RSI-Ground Loop | 46 | 26 | 40.30785 | -119 | 25 | 43.65410 | 141.8260 | 1.0612 |
| RSI-GPS | 46 | 26 | 40.30785 | -119 | 25 | 43.65410 | 141.8270 | 1.0612 |
| CBI-GPS | 46 | 26 | 40.30783 | -119 | 25 | 43.65421 | 141.8390 | 1.0612 |
| <i>BT/VE3</i> | | | | | | | | |
| IMTEC | 46 | 26 | 39.93653 | -119 | 25 | 44.39319 | 141.8402 | 1.0612 |
| RSI-Ground Loop | 46 | 26 | 39.93649 | -119 | 25 | 44.39314 | 141.8342 | 1.0612 |
| RSI-GPS | 46 | 26 | 39.93649 | -119 | 25 | 44.39314 | 141.8310 | 1.0612 |
| CBI-GPS | 46 | 26 | 39.93653 | -119 | 25 | 44.39319 | 141.8450 | 1.0612 |

Table 3: Cardinal Marker Survey Data for Hanford

| <i>Marker ID Source</i> | <i>Latitude[N]</i> | | | <i>Longitude[W]</i> | | | <i>Ellipsoidal height of marker</i> | <i>Design height of beam centerline above marker elevation</i> |
|-----------------------------|--------------------|----|----------|---------------------|----|----------|---------------------------------------------|----------------------------------------------------------------------------|
| | ° | ' | " | ° | ' | " | <i>m</i> | <i>m</i> |
| <i>BT/VE4</i> | | | | | | | | |
| IMTEC | 46 | 26 | 2.57842 | -119 | 26 | 58.70927 | 142.7882 | 1.0592 |
| RSI-Ground Loop | 46 | 26 | 2.57842 | -119 | 26 | 58.70928 | 142.7932 | 1.0592 |
| RSI-GPS | 46 | 26 | 2.57842 | -119 | 26 | 58.70928 | 142.7980 | 1.0592 |
| CBI-GPS | 46 | 26 | 2.57842 | -119 | 26 | 58.70928 | 142.7980 | 1.0592 |
| <i>BT/VE5</i> | | | | | | | | |
| IMTEC | 46 | 27 | 19.73298 | -119 | 24 | 28.83263 | 141.4677 | 1.0612 |
| RSI-Ground Loop | 46 | 27 | 19.73310 | -119 | 24 | 28.83270 | 141.4677 | 1.0612 |
| RSI-GPS | 46 | 27 | 19.73310 | -119 | 24 | 28.83270 | 141.4690 | 1.0612 |
| CBI-GPS | 46 | 27 | 19.73298 | -119 | 24 | 28.83263 | 141.4650 | 1.0612 |
| <i>BT/VE6</i> | | | | | | | | |
| IMTEC | 46 | 28 | 11.12085 | -119 | 25 | 22.87130 | 140.5684 | 1.0569 |
| RSI-Ground Loop | 46 | 28 | 11.12114 | -119 | 25 | 22.87150 | 140.5714 | 1.0569 |
| RSI-GPS | 46 | 28 | 11.12114 | -119 | 25 | 22.87150 | 140.5650 | 1.0569 |
| <i>BT/VE7</i> | | | | | | | | |
| IMTEC | 46 | 28 | 11.63174 | -119 | 25 | 23.40854 | 140.5626 | 1.0579 |
| RSI-Ground Loop | 46 | 28 | 11.63199 | -119 | 25 | 23.40886 | 140.5686 | 1.0579 |
| RSI-GPS | 46 | 28 | 11.63199 | -119 | 25 | 23.40886 | 140.5600 | 1.0579 |
| <i>BT/VE8</i> | | | | | | | | |
| IMTEC | 46 | 29 | 3.01234 | -119 | 26 | 17.47572 | 140.2633 | 1.0632 |
| RSI-Ground Loop | 46 | 29 | 3.01263 | -119 | 26 | 17.47612 | 140.2763 | 1.0632 |
| RSI-GPS | 46 | 29 | 3.01263 | -119 | 26 | 17.47612 | 140.2640 | 1.0632 |
| CBI-GPS | 46 | 29 | 3.01234 | -119 | 26 | 17.47572 | 140.2680 | 1.0632 |

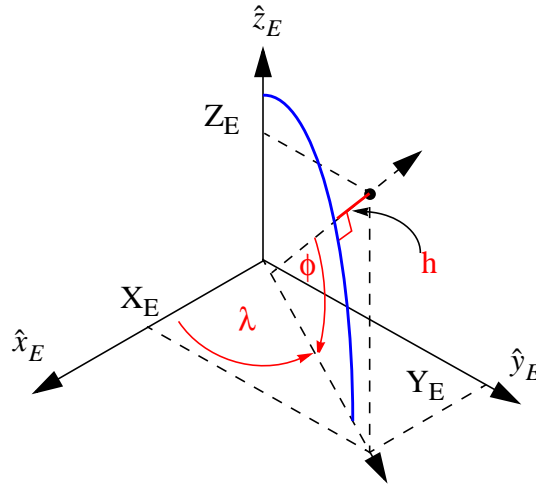
2.1 Fit to the Survey Data

A *global orthonormal coordinate system* was determined which has its \hat{x}_G and \hat{y}_G axes along best fit lines defined by the markers along the arms. The \hat{z}_G axis is defined by the cross product:

$$\hat{z}_G = \hat{x}_G \times \hat{y}_G.$$

The data of Table 3 were converted to the earth-fixed Cartesian system, $\{\hat{x}_E, \hat{y}_E, \hat{z}_E\}$, used for geodetic work. In this system, \hat{x}_E pierces the earth surface at $\{\phi, \lambda\} = \{000, 000\}$, \hat{y}_E pierces the earth's surface at $\{\phi, \lambda\} = \{000, 090E\}$, and \hat{z}_E pierces the earth's surface at $\{\phi, \lambda\} = \{090N, 000\}$. The relationship between the coordinates of a point $\{h, \phi, \lambda\}$ and $\{X_E, Y_E, Z_E\}$ is depicted in **Figure 1**.

Figure 1: Geodetic and Earth-Fixed Coordinates



The functional relationships are given by:

$$X_E = ((R[\phi] + h) \cos \phi \cos \lambda)$$

$$Y_E = (R[\phi] + h) \cos \phi \sin \lambda$$

$$Z_E = ([1 - \epsilon^2] R[\phi] + h) \sin \phi$$

The earth model WGS-84, is described by an oblate ellipsoid with its semi-minor axis, $b = 6356752.314$ m, along \hat{z}_E , semi-major axis with value $a = 6378137$ m, and eccentricity giving $[1 - \epsilon^2] = 0.993306$. $R[\phi]$ is the local radius of curvature of the ellipsoid at latitude ϕ :

$$R[\phi] = \frac{a^2}{a^2 \cos^2 \phi + b^2 \sin^2 \phi}$$

Note that in the geodetic model the vector h is aligned along the local surface normal. Consequently its extension to the equatorial plane does not, in general, intersect the origin.

The set of orthonormal axes which best describes the Cartesian data for the markers were determined by a χ^2 minimization of the transverse (2D) residuals of the marker positions from the best-fit axes. There are six degrees of freedom for the fit: 3 translational and three rotational. These were

chosen as:

- **three** coordinates for the vertex, $\{X_v, Y_v, Z_v\}$;
- **two** direction cosines for one axis, $\{n_{xx}, n_{xy}, 1\}$; the z component was fixed.
- **one** direction cosine for the remaining axis (the orientation of the remaining axis in the plane normal to the first axis), $\left\{n_{yx}, \frac{-(n_{xx}n_{yx} + 1)}{n_{xy}}, 1\right\}$; this is done by fitting the x component of the second normal, constraining the y and z components.

The errors associated with many of the measured data were not reported in the surveys. Therefore the fitting procedure assumed equal weights for all data: the χ^2 optimization was reduced to a least squares minimization.

The 3-axis RMS residual for the best fit was 0.0053 m. This fit gives parameter values listed in **Figure 4**.

Table 4: Parameters resulting from best fit to the survey data for Hanford, WA

| Parameter | Value | Estimated Error | Units |
|-------------|---------------------------------------------------------------------------------------------------------------------------|--------------------------|---------------|
| Vertex | Global $\{\hat{x}_G, \hat{y}_G, \hat{z}_G\}: \{0,0,0\}$ | {0.0064, 0.0073, 0.0050} | m |
| | Geodetic $\{h, \phi, \lambda\}: \{142.554, \{46,27,18.528\}, \{-119,24,27.5657\}\}$ | - | {m, deg, deg} |
| | Earth-fixed $\{\hat{x}_E, \hat{y}_E, \hat{z}_E\}: \{-2.1614149 \cdot 10^6, -3.8346952 \cdot 10^6, 4.6003502 \cdot 10^6\}$ | {0.0066, 0.0057, 0.0054} | m |
| \hat{x}_G | Global $\{\hat{x}_G, \hat{y}_G, \hat{z}_G\}: \{1,0,0\}$ | - | |
| | Earth-fixed $\{\hat{x}_E, \hat{y}_E, \hat{z}_E\}: \{-0.223892, 0.799831, 0.556905\}$ | - | |
| | Compass Direction: N35.9994° W (ref. geodetic north) ^a | $1.93 \cdot 10^{-6}$ | radian |
| | Angle <i>below</i> local horizontal at Vertex: $6.195 \cdot 10^{-4}$ | $2.73 \cdot 10^{-6}$ | radian |
| \hat{y}_G | Global $\{\hat{x}_G, \hat{y}_G, \hat{z}_G\}: \{0,1,0\}$ | | |
| | Earth-fixed $\{\hat{x}_E, \hat{y}_E, \hat{z}_E\}: \{-0.913978, 0.0260945, -0.404923\}$ | | |
| | Compass Direction: S54.0006° W (see footnote a) | $1.93 \cdot 10^{-6}$ | radian |
| | Angle <i>above</i> local horizontal at Vertex: $1.25 \cdot 10^{-5}$ | $2.73 \cdot 10^{-6}$ | radian |

Table 4: Parameters resulting from best fit to the survey data for Hanford, WA

| <i>Parameter</i> | <i>Value</i> | <i>Estimated Error</i> | <i>Units</i> |
|------------------|------------------------------------------------------------------------------------|------------------------|--------------|
| \hat{z}_G | Global $\{\hat{x}_G, \hat{y}_G, \hat{z}_G\}$: {0,0,1} | | |
| | Earth-fixed $\{\hat{x}_E, \hat{y}_E, \hat{z}_E\}$: {-0.338402,-0.599658,0.725186} | | |
| | Deviation from zenith at vertex: $6.195 \cdot 10^{-4}$, toward \hat{x}_G | $2.73 \cdot 10^{-6}$ | radian |

- a. Site drawings call for arms to run N36.8° W and S53.2° W; these are referred to the WA state plane coordinates (northing & easting). Geodetic north is 47'39" (~0.8 °) W of grid north at the vertex.

Location of as-built BT/VE markers relative to global coordinate system

Using the coordinate system described above, the positions for each of the 8 BT/VE interface markers were determined by averaging the residuals from multiple measurements of individual markers. **Table 5** presents the results.

Table 5: Global coordinate positions of as-built BT/VE interface markers

| Marker ID | X_G | Y_G | Z_G |
|-----------|-----------|-----------|---------|
| BT/VE 1 | 0.0000 | 46.0020 | -1.0572 |
| BT/VE 2 | -0.0011 | 2007.5000 | -1.0639 |
| BT/VE 3 | -0.00052 | 2027.0000 | -1.0642 |
| BT/VE 4 | -0.0012 | 3988.5000 | -1.0564 |
| BT/VE 5 | 45.9970 | 0.0028 | -1.0588 |
| BT/VE 6 | 2007.5000 | 0.0010 | -1.0585 |
| BT/VE 7 | 2027.0000 | -0.0004 | -1.0571 |
| BT/VE 8 | 3988.5000 | -0.0023 | -1.0630 |

The scatter of the residuals is presented graphically in **Figure 2** and **Figure 3**. **Figure 2** presents the scatter in the plane normal to the axis for each arm. There is an apparent greater right-left scatter along the X arm. This is a result of the fact that the best description of the marker positions corresponds to two axes which are not exactly orthogonal: an optimization without imposing the orthogonality constraint between the best fit lines results in axes having an included angle ~ 1.3 microradians greater than 90 degrees. This fact may be seen in the lower panels of **Figure 3** which

present residuals in the horizontal plane as a function of their position along the arms.

Figure 2: Scatter plots of fit residuals in plane normal to global axis for Hanford, WA.

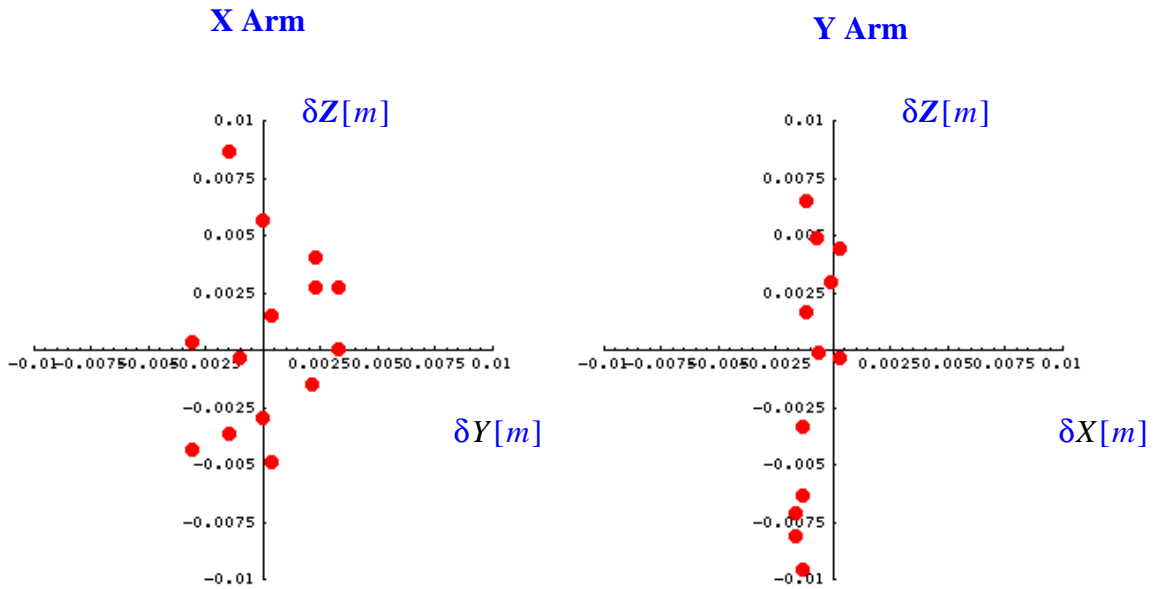
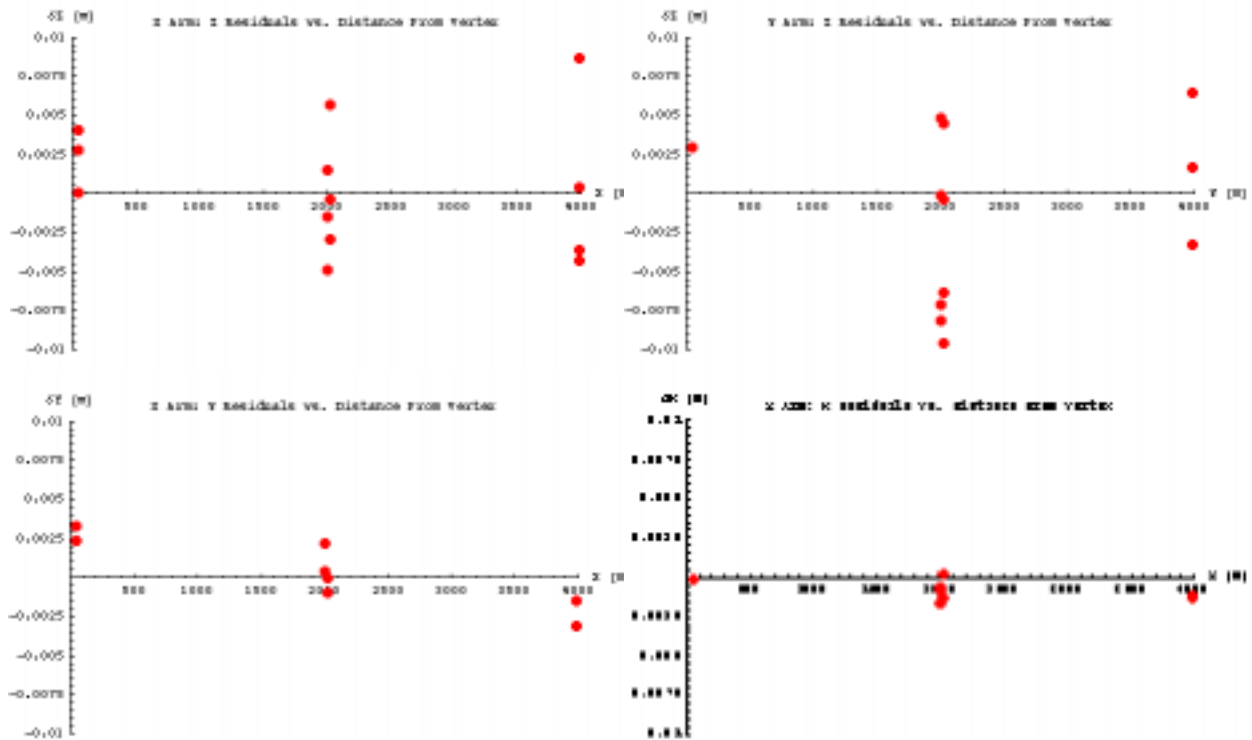


Figure 3: Dependence of residuals on distance along the arms, Hanford, WA.



2.2 Error propagators in the fits

Any error in the estimated position of the vertex results in a common mode offset to all marker positions; errors in the estimated directions of the coordinate axis result in either differential mode or common mode offsets according which orientation angle is in error and the effect on marker position is in proportion to marker distances from the vertex. This behavior is represented by the error propagation matrices presented as **Table 6**, **Table 7** and **Table 8**. Each table corresponds to one coordinate. The rows give the effects of parameter variations the eight marker locations. Vertex translational errors are referred along the global axes. Angular errors in the orientation of the axes are referred to roll, pitch and yaw of the \hat{z}_G axis. Pitch gives a common mode up/down displacement for all markers. This rotation is denoted by θ_{CM} which arises from infinitesimal rotational errors about the axis

$$\hat{n}_{CM} = \frac{\hat{y}_G - \hat{x}_G}{\sqrt{2}} ;$$

Yaw gives a differential mode up/down displacement for all markers. This rotation is denoted by θ_{DM} which arises from infinitesimal rotational errors about the axis

$$\hat{n}_{DM} = \frac{\hat{y}_G + \hat{x}_G}{\sqrt{2}}$$

θ_z corresponds to an error in marker positions which arises from infinitesimal rotational errors about the axis \hat{z}_G . The roll pitch and yaw axes are depicted in **Figure 4**.

Figure 4: Pitch, yaw, and roll axes for the orientation error analysis.

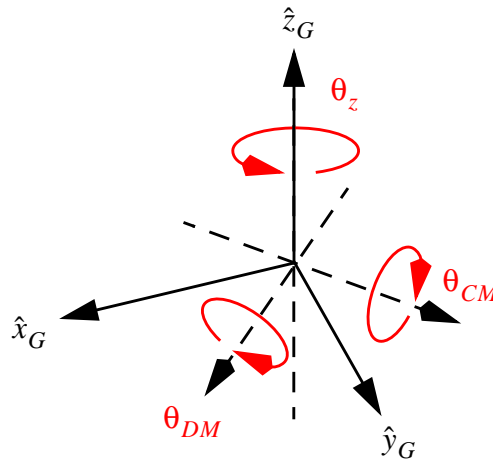


Table 6: Sensitivity matrix for the X_G coordinate for BTVE markers

| Marker ID | $\frac{\partial}{\partial V_x}$ [m/m] | $\frac{\partial}{\partial V_y}$ [m/m] | $\frac{\partial}{\partial V_z}$ [m/m] | $\frac{\partial}{\partial \theta_{CM}}$ [m/rad] | $\frac{\partial}{\partial \theta_{DM}}$ [m/rad] | $\frac{\partial}{\partial \theta_z}$ [m/rad] |
|-----------|------------------------------------------|------------------------------------------|------------------------------------------|----------------------------------------------------|----------------------------------------------------|-------------------------------------------------|
| $BTVE1_x$ | -0.224 | 0.800 | 0.557 | -0.002091 | -0.002091 | 46.002 |
| $BTVE2_x$ | -0.224 | 0.800 | 0.557 | , 0.001873 | 0.001873 | 2007.502 |
| $BTVE3_x$ | -0.224 | 0.800 | 0.557 | , 0.002090 | 0.002090 | 2027.003 |
| $BTVE4_x$ | -0.224 | 0.800 | 0.557 | -0.001999 | -0.001999 | 3988.504 |
| $BTVE5_x$ | -0.224 | 0.800 | 0.557 | -0.001695 | -0.001695 | 0.00279 |
| $BTVE6_x$ | -0.224 | 0.800 | 0.557 | , 0.001135 | 0.001135 | 0.000963 |
| $BTVE7_x$ | -0.224 | 0.800 | 0.557 | -0.0005588 | -0.0005588 | -0.000356 |
| $BTVE8_x$ | -0.224 | 0.800 | 0.557 | -0.0001960 | -0.0001960 | -0.00230 |

Table 7: Sensitivity matrix for the Y_G coordinate for BTVE markers

| Marker ID | $\frac{\partial}{\partial V_x}$ [m/m] | $\frac{\partial}{\partial V_y}$ [m/m] | $\frac{\partial}{\partial V_z}$ [m/m] | $\frac{\partial}{\partial \theta_{CM}}$ [m/rad] | $\frac{\partial}{\partial \theta_{DM}}$ [m/rad] | $\frac{\partial}{\partial \theta_z}$ [m/rad] |
|-----------|------------------------------------------|------------------------------------------|------------------------------------------|----------------------------------------------------|----------------------------------------------------|-------------------------------------------------|
| $BTVE1_y$ | -0.914 | 0.0261 | -0.405 | -0.002091 | 0.002091 | 0.0000426 |
| $BTVE2_y$ | -0.914 | 0.0261 | -0.405 | 0.001873 | -0.001873 | 0.00111 |
| $BTVE3_y$ | -0.914 | 0.0261 | -0.405 | 0.002090 | -0.002090 | 0.000519 |
| $BTVE4_y$ | -0.914 | 0.0261 | -0.405 | -0.001999 | 0.001999 | 0.001217 |
| $BTVE5_y$ | -0.914 | 0.0261 | -0.405 | -0.001695 | 0.001695 | -45.997 |
| $BTVE6_y$ | -0.914 | 0.0261 | -0.405 | 0.001135 | -0.001135 | -2007.500 |
| $BTVE7_y$ | -0.914 | 0.0261 | -0.405 | -0.0005588 | 0.0005588 | -2027.000 |
| $BTVE8_y$ | -0.914 | 0.0261 | -0.405 | -0.0001960 | 0.0001960 | -3988.497 |

Table 8: Sensitivity matrix for the Z_G coordinate for BTVE markers

| Marker ID | $\frac{\partial}{\partial V_x}$ [m/m] | $\frac{\partial}{\partial V_y}$ [m/m] | $\frac{\partial}{\partial V_z}$ [m/m] | $\frac{\partial}{\partial \theta_{CM}}$ [m/rad] | $\frac{\partial}{\partial \theta_{DM}}$ [m/rad] | $\frac{\partial}{\partial \theta_z}$ [m/rad] |
|-----------|------------------------------------------|------------------------------------------|------------------------------------------|----------------------------------------------------|----------------------------------------------------|-------------------------------------------------|
| $BTVE1_z$ | -0.338 | -0.600 | 0.725 | 32.528 | -32.528 | 0 |
| $BTVE2_z$ | -0.338 | -0.600 | 0.725 | 1419.517 | -1419.519 | 0 |
| $BTVE3_z$ | -0.338 | -0.600 | 0.725 | 1433.307 | -1433.308 | 0 |
| $BTVE4_z$ | -0.338 | -0.600 | 0.725 | 2820.298 | -2820.299 | 0 |
| $BTVE5_z$ | -0.338 | -0.600 | 0.725 | 32.527 | 32.523 | 0 |
| $BTVE6_z$ | -0.338 | -0.600 | 0.725 | 1419.517 | 1419.516 | 0 |
| $BTVE7_z$ | -0.338 | -0.600 | 0.725 | 1433.305 | 1433.306 | 0 |
| $BTVE8_z$ | -0.338 | -0.600 | 0.725 | 2820.291 | 2820.295 | 0 |

Table 9 presents uncertainties in vertex position and axis orientations. The uncertainties were defined as the amount of parameter variation which results in a doubling of the RMS residuals from the minimum value 0.0053 m. The vector in **Table 9** may be multiplied by each of the previous tables to obtain the (correlated) errors in marker positions.

Table 9: Uncertainties in fitted parameters. Changing the best fit values by these amounts result in a doubling of the RMS residual fitting error.

| Parameter | Error |
|---------------|--------------------------|
| V_x | 0.0064 m |
| V_x | 0.0073 m |
| V_x | 0.0050 m |
| θ_{CM} | $2.73 \cdot 10^{-6}$ rad |
| θ_{DM} | $2.73 \cdot 10^{-6}$ rad |
| θ_z | $1.93 \cdot 10^{-6}$ rad |

2.3 Hanford Local Coordinate Systems in each station

Table 10, Table 11, Table 12, Table 13 and **Table 14** present the direction cosines between the global coordinate system and the local coordinate systems for each station. The local coordinates are defined in LIGO-L950128 and LIGO-T950004 listed in **Table 1**.

Table 10: Hanford Vertex Global-Local System Direction Cosines

| | \hat{x}_L | \hat{y}_L | \hat{z}_L |
|-------------|-----------------------------|-----------------------------|-----------------------------|
| \hat{x}_G | $1 - 1.91886 \cdot 10^{-7}$ | 0 | -0.00061949 |
| \hat{y}_G | $7.7333 \cdot 10^{-9}$ | $1 - 7.7916 \cdot 10^{-11}$ | 0.0000124832 |
| \hat{z}_G | 0.00061949 | -0.0000124832 | $1 - 1.91964 \cdot 10^{-7}$ |

Table 11: Hanford X End Station (d= 4000m) Global-Local System Direction Cosines

| | \hat{x}_L | \hat{y}_L | \hat{z}_L |
|-------------|------------------------------|-----------------------------|-----------------------------|
| \hat{x}_G | $1 - 3.07241 \cdot 10^{-11}$ | 0 | $7.8389 \cdot 10^{-6}$ |
| \hat{y}_G | 0 | $1 - 6.6491 \cdot 10^{-11}$ | 0.0000115318 |
| \hat{z}_G | $-7.8389 \cdot 10^{-6}$ | -0.0000115318 | $1 - 9.7215 \cdot 10^{-11}$ |

Table 12: Hanford Y End Station (d= 4000m) Global-Local System Direction Cosines

| | \hat{x}_L | \hat{y}_L | \hat{z}_L |
|-------------|-----------------------------|-----------------------------|----------------------------|
| \hat{x}_G | $1 - 1.92477 \cdot 10^{-7}$ | 0 | -0.00062045 |
| \hat{y}_G | $3.9659 \cdot 10^{-7}$ | $1 - 2.04288 \cdot 10^{-7}$ | 0.00063920 |
| \hat{z}_G | 0.00062045 | -0.00063920 | $1 - 3.9677 \cdot 10^{-7}$ |

Table 13: Hanford X Mid-Station (d = 2000m) Global-Local System Direction Cosines

| | \hat{x}_L | \hat{y}_L | \hat{z}_L |
|-------------|----------------------------|-----------------------------|----------------------------|
| \hat{x}_G | $1 - 4.6765 \cdot 10^{-8}$ | 0 | -0.000305827 |
| \hat{y}_G | $3.6722 \cdot 10^{-9}$ | $1 - 7.2090 \cdot 10^{-11}$ | 0.0000120075 |
| \hat{z}_G | 0.000305827 | -0.0000120075 | $1 - 4.6837 \cdot 10^{-8}$ |

Table 14: Hanford Y Mid-Station (d = 2000m) Global-Local System Direction Cosines

| | \hat{x}_L | \hat{y}_L | \hat{z}_L |
|-------------|-----------------------------|----------------------------|-----------------------------|
| \hat{x}_G | $1 - 1.92182 \cdot 10^{-7}$ | 0 | -0.00061997 |
| \hat{y}_G | $2.02012 \cdot 10^{-7}$ | $1 - 5.3086 \cdot 10^{-8}$ | 0.00032584 |
| \hat{z}_G | 0.00061997 | -0.00032584 | $1 - 2.45268 \cdot 10^{-7}$ |

3 LIVINGSTON SURVEY DATA

The alignment of the Livingston beam tube arms proceeded in a different manner from what was done at Hanford. Excellent experience with the Beam Tube contractor in Hanford, combined with correspondingly negative experience with the surveying contractor in Livingston led to a decision to use the CB&I alignment database as the primary basis for determining the best estimate of the beam tube alignment. Although similar BT/VE interface markers exist for Livingston, it is believed that better accuracy could be achieved by using 64 control points measured by CB&I directly on the beam tube with GPS methods. This was possible in Livingston because CB&I bored perforations along the top of the Beam Tube Enclosure, and these allowed directly contacting survey measurements to be made of the beam tube. These data were used for the analysis reported here.

For completeness, the BTVE interface markers that were installed in Livingston are also reported. These points defined the interface positions for the beam tube (BT) and vacuum equipment (VE)

contracts. These points are identified by suitably inscribed marks on each of six brass markers, denoted {BT/VE1, BT/VE3, BT/VE4, BT/VE5, BT/VE7, BT/VE8} (see D950021 for specifications). The design positions in global coordinates of the interface markers are given in **Table 15**. *Note that these were NOT used in the regression analysis.*

Table 15: Design values of the global coordinate positions of BT/VE interface markers

| Marker ID ^a | X_G | Y_G | Z_G |
|------------------------|----------|----------|---------------------|
| BT/VE 1 | 46.000 | 0.000 | -1.070 ^b |
| BT/VE 3 | 2017.433 | 0.000 | -1.070 |
| BT/VE 4 | 3988.500 | 0.000 | -1.070 |
| BT/VE 5 | 0.000 | 46.000 | -1.070 |
| BT/VE 7 | 0.000 | 2017.433 | -1.070 |
| BT/VE 8 | 0.000 | 3988.500 | -1.070 |

- a. The same nomenclature for the BT/VE markers was used as at Hanford. Since Livingston has no mid-stations, only one marker was placed at the 2km points. Hence BT/VE 2 and BT/VE 6 do not exist.
- b. The design for the BT centerline was to be 1.070 m above the finished slab.

BT/VE1 - BT/VE4 lie along the Y arm and BT/VE5 - BT/VE8 are arranged along the X arm.

During the course of constructing the beam tubes, the markers were surveyed a number of times by the Beam Tube contractor (CB&I) and by a professional surveying company (JSB). **Table 16** presents the survey results for the six BT/VE markers. The markers were placed on the as-built beam tube slabs. Their heights are affected by slight irregularities in the slab finish. After the first survey by JSB, LIGO determined the best estimate (at that time) for the vertical offsets above each of the markers where the beam tube centerline should be located. The last column in the table shows these vertical offsets.

Table 16: Cardinal Marker Survey Data for Livingston

| <i>Marker ID Source</i> | <i>Latitude[N]</i> | | | <i>Longitude[W]</i> | | | <i>Ellipsoidal height of marker</i> | <i>Design height of beam centerline above marker elevation</i> |
|-----------------------------|--------------------|----|-----------|---------------------|----|-----------|---------------------------------------------|----------------------------------------------------------------------------|
| | ° | ' | " | ° | ' | " | <i>m</i> | <i>m</i> |
| <i>BT/VE1</i> | | | | | | | | |
| JSB ^a | 30 | 33 | 44.996494 | 90 | 46 | 26.740208 | -7.638 | 1.034 ^b |
| JSB ^c | 30 | 33 | 44.996471 | 90 | 46 | 26.739908 | -7.638 | - |
| <i>BT/VE3</i> | | | | | | | | |
| JSB ^a | 30 | 32 | 44.013807 | 90 | 46 | 4.232303 | -8.549 | 1.061 ^b |
| JSB ^c | 30 | 32 | 44.013807 | 90 | 46 | 4.232303 | -8.549 | - |

Table 16: Cardinal Marker Survey Data for Livingston

| Marker ID Source | <i>Latitude[N]</i> | | | <i>Longitude[W]</i> | | | <i>Ellipsoidal height of marker</i> | <i>Design height of beam centerline above marker elevation</i> |
|-----------------------------|--------------------|----|-----------|---------------------|----|-----------|---------------------------------------------|----------------------------------------------------------------------------|
| | ° | ' | " | ° | ' | " | m | m |
| <i>BT/VE4</i> | | | | | | | | |
| JSB ^a | 30 | 31 | 43.041625 | 90 | 45 | 41.736474 | -8.825 | 1.066 ^b |
| JSB ^c | 30 | 31 | 43.041709 | 90 | 45 | 41.736110 | -8.825 | - |
| <i>BT/VE5</i> | | | | | | | | |
| JSB ^d | 30 | 33 | 45.964860 | 90 | 46 | 28.909760 | -7.653 | 1.059 ^b |
| JSB ^c | 30 | 33 | 45.964752 | 90 | 46 | 28.909220 | -7.653 | - |
| <i>BT/VE7</i> | | | | | | | | |
| JSB ^d | 30 | 32 | 44.013807 | 90 | 46 | 4.232303 | -7.943 | 1.057 ^b |
| JSB ^c | 30 | 33 | 26.478149 | 90 | 47 | 39.374652 | -7.943 | - |
| <i>BT/VE8</i> | | | | | | | | |
| JSB ^d | 30 | 33 | 6.984673 | 90 | 48 | 49.818452 | -7.652 | 1.080 ^b |
| JSB ^c | 30 | 33 | 6.984673 | 90 | 48 | 49.818452 | -7.652 | - |

- a. 1 December 1997 data, JSB LIGO-C982063-00; NOTE: *BTVE3 is identical to BTVE7, implying an error in the JSB report.*
- b. TDM LIGO-C972035-00 to CB&I
- c. April 1998 data, JSB LIGO-C982063-00.
- d. 18 December 1997 data, JSB LIGO-C982063-00; NOTE: *BTVE7 is identical to BTVE3, implying an error in the JSB report.*

Table 17 lists the 64 control points reported by CB&I as the final alignment data for the beam tube. The control points were measured directly contacting the beam tube

Table 17: Control Point CB&I Survey Data

| <i>CB&I Marker ID</i> <i>Source</i> | <i>Latitude[N]</i> | | | <i>Longitude[W]</i> | | | <i>Ellipsoidal height of BT CL</i> |
|--------------------------------------------|--------------------|----|----------|---------------------|----|----------|--------------------------------------------|
| | ° | ' | " | ° | ' | " | <i>m</i> |
| X arm, Module 1 | | | | | | | |
| 007-L-SW-7-06 | 30 | 33 | 44.84322 | 90 | 46 | 32.96651 | -6.619 |
| 013-L-SW-7-12 | 30 | 33 | 43.66847 | 90 | 46 | 37.21612 | -6.657 |
| 019-L-SW-7-18 | 30 | 33 | 42.49373 | 90 | 46 | 41.46493 | -6.682 |
| 025-L-SW-7-24 | 30 | 33 | 41.3189 | 90 | 46 | 45.71427 | -6.712 |
| 031-L-SW-7-30 | 30 | 33 | 40.14409 | 90 | 46 | 49.96287 | -6.741 |
| 037-L-SW-7-36 | 30 | 33 | 38.96912 | 90 | 46 | 54.21174 | -6.764 |
| 043-L-SW-7-42 | 30 | 33 | 37.79447 | 90 | 46 | 58.46065 | -6.787 |
| 049-L-SW-7-48 | 30 | 33 | 36.61928 | 90 | 47 | 2.70953 | -6.805 |
| 055-L-SW-7-54 | 30 | 33 | 35.44441 | 90 | 47 | 6.9584 | -6.824 |
| 061-L-SW-7-60 | 30 | 33 | 34.26942 | 90 | 47 | 11.20717 | -6.839 |
| 067-L-SW-7-66 | 30 | 33 | 33.09422 | 90 | 47 | 15.45617 | -6.85 |
| 073-L-SW-7-72 | 30 | 33 | 31.91912 | 90 | 47 | 19.70463 | -6.864 |
| 079-L-SW-7-78 | 30 | 33 | 30.7442 | 90 | 47 | 23.95327 | -6.873 |
| 085-L-SW-7-84 | 30 | 33 | 29.56901 | 90 | 47 | 28.20187 | -6.879 |
| 091-L-SW-7-90 | 30 | 33 | 28.39329 | 90 | 47 | 32.45168 | -6.881 |
| 095-L-SW-7-94 | 30 | 33 | 27.60975 | 90 | 47 | 35.28413 | -6.884 |
| X arm, Module 2 | | | | | | | |
| 007-L-SW-8-06 | 30 | 33 | 25.35021 | 90 | 47 | 43.45273 | -6.884 |
| 011-L-SW-8-10 | 30 | 33 | 24.56673 | 90 | 47 | 46.28478 | -6.880 |
| 017-L-SW-8-16 | 30 | 33 | 23.39107 | 90 | 47 | 50.53357 | -6.871 |
| 023-L-SW-8-22 | 30 | 33 | 22.21583 | 90 | 47 | 54.78214 | -6.867 |
| 029-L-SW-8-28 | 30 | 33 | 21.04034 | 90 | 47 | 59.03045 | -6.853 |
| 035-L-SW-8-34 | 30 | 33 | 19.86488 | 90 | 48 | 3.27876 | -6.849 |
| 041-L-SW-8-40 | 30 | 33 | 18.68923 | 90 | 48 | 7.52733 | -6.834 |
| 047-L-SW-8-46 | 30 | 33 | 17.51372 | 90 | 48 | 11.77571 | -6.819 |
| 053-L-SW-8-52 | 30 | 33 | 16.33795 | 90 | 48 | 16.02414 | -6.797 |
| 059-L-SW-8-58 | 30 | 33 | 15.1623 | 90 | 48 | 20.27255 | -6.778 |
| 065-L-SW-8-64 | 30 | 33 | 13.98671 | 90 | 48 | 24.52062 | -6.755 |
| 071-L-SW-8-70 | 30 | 33 | 12.81112 | 90 | 48 | 28.76863 | -6.726 |
| 077-L-SW-8-76 | 30 | 33 | 11.63519 | 90 | 48 | 33.01682 | -6.701 |
| 083-L-SW-8-82 | 30 | 33 | 10.45933 | 90 | 48 | 37.26522 | -6.67 |
| 089-L-SW-8-88 | 30 | 33 | 9.28357 | 90 | 48 | 41.51372 | -6.638 |
| 095-L-SW-8-94 | 30 | 33 | 8.10749 | 90 | 48 | 45.76245 | -6.609 |

Table 17: Control Point CB&I Survey Data

| <i>CB&I Marker ID</i> <i>Source</i> | <i>Latitude[N]</i> | | | <i>Longitude[W]</i> | | | <i>Ellipsoidal height of BT CL</i> |
|--------------------------------------------|--------------------|----|----------|---------------------|----|----------|------------------------------------|
| | ° | ' | '' | ° | ' | '' | <i>m</i> |
| Y arm, Module1 | | | | | | | |
| -L-SE-5-06 | 30 | 33 | 41.51672 | 90 | 46 | 25.45574 | -6.666 |
| 013-L-SE-5-12 | 30 | 33 | 37.80886 | 90 | 46 | 24.08704 | -6.741 |
| 019-L-SE-5-18 | 30 | 33 | 34.13159 | 90 | 46 | 22.72963 | -6.805 |
| 025-L-SE-5-24 | 30 | 33 | 30.45399 | 90 | 46 | 21.37209 | -6.869 |
| 031-L-SE-5-30 | 30 | 33 | 26.77698 | 90 | 46 | 20.01464 | -6.931 |
| 037-L-SE-5-36 | 30 | 33 | 23.09977 | 90 | 46 | 18.65745 | -6.985 |
| 043-L-SE-5-42 | 30 | 33 | 19.42326 | 90 | 46 | 17.30056 | -7.045 |
| 049-L-SE-5-48 | 30 | 33 | 15.74548 | 90 | 46 | 15.94307 | -7.102 |
| 055-L-SE-5-54 | 30 | 33 | 12.06884 | 90 | 46 | 14.58607 | -7.158 |
| 061-L-SE-5-60 | 30 | 33 | 8.39187 | 90 | 46 | 13.22903 | -7.205 |
| 067-L-SE-5-66 | 30 | 33 | 4.71473 | 90 | 46 | 11.87175 | -7.256 |
| 073-L-SE-5-72 | 30 | 33 | 1.03757 | 90 | 46 | 10.51468 | -7.296 |
| 079-L-SE-5-78 | 30 | 32 | 57.36069 | 90 | 46 | 9.15775 | -7.345 |
| 085-L-SE-5-84 | 30 | 32 | 53.68373 | 90 | 46 | 7.80083 | -7.387 |
| 091-L-SE-5-90 | 30 | 32 | 50.0063 | 90 | 46 | 6.44356 | -7.426 |
| 095-L-SE-5-94 | 30 | 32 | 47.55538 | 90 | 46 | 5.53913 | -7.451 |
| Y arm, Module 2 | | | | | | | |
| 007-L-SE-6-06 | 30 | 32 | 40.48398 | 90 | 46 | 2.92976 | -7.518 |
| 011-L-SE-6-10 | 30 | 32 | 38.03278 | 90 | 46 | 2.02525 | -7.54 |
| 017-L-SE-6-16 | 30 | 32 | 34.35561 | 90 | 46 | 0.66832 | -7.57 |
| 023-L-SE-6-22 | 30 | 32 | 30.67897 | 90 | 45 | 59.31167 | -7.592 |
| 029-L-SE-6-28 | 30 | 32 | 27.00148 | 90 | 45 | 57.9548 | -7.624 |
| 035-L-SE-6-34 | 30 | 32 | 23.32402 | 90 | 45 | 56.59774 | -7.647 |
| 041-L-SE-6-40 | 30 | 32 | 19.64763 | 90 | 45 | 55.24134 | -7.671 |
| 047-L-SE-6-46 | 30 | 32 | 15.96996 | 90 | 45 | 53.88442 | -7.687 |
| 053-L-SE-6-52 | 30 | 32 | 12.29286 | 90 | 45 | 52.5279 | -7.703 |
| 059-L-SE-6-58 | 30 | 32 | 8.61604 | 90 | 45 | 51.17127 | -7.716 |
| 065-L-SE-6-64 | 30 | 32 | 4.9388 | 90 | 45 | 49.81468 | -7.728 |
| 071-L-SE-6-70 | 30 | 32 | 1.26155 | 90 | 45 | 48.45788 | -7.739 |
| 077-L-SE-6-76 | 30 | 31 | 57.58426 | 90 | 45 | 47.10137 | -7.746 |
| 083-L-SE-6-82 | 30 | 31 | 53.90631 | 90 | 45 | 45.74429 | -7.753 |
| 089-L-SE-6-88 | 30 | 31 | 50.22968 | 90 | 45 | 44.388 | -7.759 |
| 095-L-SE-6-94 | 30 | 31 | 46.55246 | 90 | 45 | 43.03153 | -7.755 |

The global coordinate axes were determined by fitting two orthogonal axes going through the data.

3.1 Fit to the Survey Data

Refer to **Section 2.1** for the details of the fitting procedure. Briefly, the data of **Table 17** were converted to the earth-fixed Cartesian system, $\{\hat{x}_E, \hat{y}_E, \hat{z}_E\}$. The earth model WGS-84 was used for transformation. The set of orthonormal axes which best describes the Courtesan data for the mark-

ers were determined by a χ^2 minimization of the transverse (2D) residuals of the control points. There are six degrees of freedom for the fit: 3 translational and three rotational. These were chosen as:

- **three** coordinates for the vertex, $\{X_v, Y_v, Z_v\}$;
- **two** direction cosines for one axis, $\{n_{xx}, n_{xy}, 1\}$; the z component was fixed.
- **one** direction cosine for the remaining axis (the orientation of the remaining axis in the plane normal to the first axis), $\left\{n_{yx}, \frac{-(n_{xx}n_{yx} + 1)}{n_{xy}}, 1\right\}$; this is done by fitting the x component of the second normal, constraining the y and z components.

The errors associated with the measured data were not reported in the survey; however experience has shown that the general accuracy CB&I was able to achieve using GPS is typically 0.005 m RMS (3-axis). The fitting procedure assumed equal weights for all data: the χ^2 optimization was reduced to a least squares minimization.

In fact, the 3-axis RMS residual for the best fit was 0.0040 m. This fit gives parameter values listed in **Table 18**.

Table 18: Parameters resulting from best fit to the survey data for Livingston, LA

| Parameter | Value | Estimated Error | Units |
|-------------|--------------------------------------------------------------------------------------------------------------------|-----------------------|---------------|
| Vertex | Global $\{\hat{x}_G, \hat{y}_G, \hat{z}_G\}: \{0,0,0\}$ | {.0062, .0055, .0041} | m |
| | Geodetic $\{h, \phi, \lambda\}: \{-6.574, \{30,33,46.4196\}, \{-90,46,27.2654\}\}$ | - | {m, deg, deg} |
| | Earth-fixed $\{\hat{x}_E, \hat{y}_E, \hat{z}_E\}: \{-74276.044, -5.496283721 \cdot 10^6, 3.224257018 \cdot 10^6\}$ | {.0062, .0055, .0041} | m |
| \hat{x}_G | Global $\{\hat{x}_G, \hat{y}_G, \hat{z}_G\}: \{1,0,0\}$ | - | |
| | Earth-fixed $\{\hat{x}_E, \hat{y}_E, \hat{z}_E\}: \{-0.954574, -0.14158, -0.262189\}$ | - | |
| | Compass Direction: $S72.2835^\circ$ W (ref. geodetic north) ^a | $1.73 \cdot 10^{-6}$ | radian |
| | Angle <i>below</i> local horizontal at Vertex: $3.121 \cdot 10^{-4}$ | $2.44 \cdot 10^{-6}$ | radian |
| \hat{y}_G | Global $\{\hat{x}_G, \hat{y}_G, \hat{z}_G\}: \{0,1,0\}$ | - | |
| | Earth-fixed $\{\hat{x}_E, \hat{y}_E, \hat{z}_E\}: \{0.297741, -0.48791, -0.820545\}$ | - | |
| | Compass Direction: $S17.7165^\circ$ E (see footnote a) | $1.73 \cdot 10^{-6}$ | radian |
| | Angle <i>below</i> local horizontal at Vertex: $6.107 \cdot 10^{-4}$ | $2.44 \cdot 10^{-6}$ | radian |

Table 18: Parameters resulting from best fit to the survey data for Livingston, LA

| <i>Parameter</i> | <i>Value</i> | <i>Estimated Error</i> | <i>Units</i> |
|------------------|------------------------------------------------------------------------------------------------------------------------------|------------------------|--------------|
| \hat{z}_G | Global $\{\hat{x}_G, \hat{y}_G, \hat{z}_G\}: \{0,0,1\}$ | - | |
| | Earth-fixed $\{\hat{x}_E, \hat{y}_E, \hat{z}_E\}: \{-0.0117515, -0.861335, 0.507901\}$ | - | |
| | Deviation from zenith at vertex, toward \hat{x}_G : $3.121 \cdot 10^{-4}$ toward \hat{y}_G : $6.107 \cdot 10^{-4}$ | $2.44 \cdot 10^{-6}$ | radian |

- a. Site drawings call for arms to run $S72^\circ W$ and $S18^\circ E$; these are referred to the LA state plane coordinates (northing & easting). Geodetic north is $17' 1''$ ($\sim 0.28^\circ$) W of grid north at the vertex.

Location of as-built BT/VE markers relative to global coordinate system

Using the coordinate system described above, the positions for each of the 6 BT/VE interface markers were determined by averaging the residuals from multiple measurements of individual markers. **Table 19** presents the results.

Table 19: Global coordinate positions of as-built BT/VE interface markers

| Marker ID | X_G | Y_G | Z_G |
|-----------|------------|------------|------------|
| BT/VE 1 | TBD | TBD | TBD |
| BT/VE 2 | TBD | TBD | TBD |
| BT/VE 4 | TBD | TBD | TBD |
| BT/VE 5 | TBD | TBD | TBD |
| BT/VE 6 | TBD | TBD | TBD |
| BT/VE 8 | TBD | TBD | TBD |

The positions of the 64 CB&I control points relative to the global coordinate system are listed in **Table 20**.

Table 20: Global coordinate positions of CB&I control points, meters

| CB&I Marker ID | X_G | Y_G | Z_G |
|-------------------|----------|--------|--------|
| X arm | | | |
| 007-L-SW-7-06 | 159.498 | 0.007 | 0.002 |
| 013-L-SW-7-12 | 278.385 | 0.003 | -0.003 |
| 019-L-SW-7-18 | 397.252 | 0.004 | 0.003 |
| 025-L-SW-7-24 | 516.133 | 0.001 | 0.001 |
| 031-L-SW-7-30 | 634.996 | 0.003 | -0.001 |
| 037-L-SW-7-36 | 753.868 | 0.006 | 0.000 |
| 043-L-SW-7-42 | 872.738 | -0.002 | -0.001 |
| 049-L-SW-7-48 | 991.613 | 0.004 | 0.001 |
| 055-L-SW-7-54 | 1110.485 | 0.000 | -0.001 |
| 061-L-SW-7-60 | 1229.356 | -0.001 | -0.001 |
| 067-L-SW-7-66 | 1348.235 | 0.001 | 0.002 |
| 073-L-SW-7-72 | 1467.100 | 0.002 | -0.002 |
| 079-L-SW-7-78 | 1585.967 | -0.004 | -0.002 |
| 085-L-SW-7-84 | 1704.837 | -0.003 | -0.001 |
| 091-L-SW-7-90 | 1823.743 | 0.002 | 0.001 |
| 095-L-SW-7-94 | 1902.992 | 0.002 | -0.001 |
| 007-L-SW-8-06 | 2131.541 | -0.003 | -0.002 |
| 011-L-SW-8-10 | 2210.78 | -0.003 | 0.000 |
| 017-L-SW-8-16 | 2329.661 | 0.002 | 0.004 |
| 023-L-SW-8-22 | 2448.533 | -0.004 | 0.001 |
| 029-L-SW-8-28 | 2567.400 | -0.002 | 0.005 |
| 035-L-SW-8-34 | 2686.268 | -0.002 | -0.003 |
| 041-L-SW-8-40 | 2805.145 | -0.001 | -0.002 |
| 047-L-SW-8-46 | 2924.016 | -0.003 | -0.003 |
| 053-L-SW-8-52 | 3042.891 | 0.001 | 0.000 |
| 059-L-SW-8-58 | 3161.765 | 0.000 | -0.001 |
| 065-L-SW-8-64 | 3280.603 | -0.002 | -0.001 |
| 071-L-SW-8-70 | 3399.494 | -0.004 | 0.003 |
| 077-L-SW-8-76 | 3518.365 | 0.001 | 0.000 |
| 083-L-SW-8-82 | 3637.242 | 0.001 | 0.002 |
| 089-L-SW-8-88 | 3756.121 | -0.005 | 0.002 |
| 095-L-SW-8-94 | 3875.009 | -0.004 | -0.003 |

Table 20: Global coordinate positions of CB&I control points, meters

| CB&I Marker ID | X_G | Y_G | Z_G |
|-------------------|--------|----------|--------|
| Y arm | | | |
| -L-SE-5-06 | 0.006 | 158.498 | 0.002 |
| 013-L-SE-5-12 | 0.007 | 278.366 | -0.004 |
| 019-L-SE-5-18 | 0.007 | 397.245 | -0.002 |
| 025-L-SE-5-24 | 0.005 | 516.135 | -0.002 |
| 031-L-SE-5-30 | 0.000 | 635.007 | -0.002 |
| 037-L-SE-5-36 | 0.003 | 753.883 | 0.004 |
| 043-L-SE-5-42 | 0.005 | 872.736 | 0.001 |
| 049-L-SE-5-48 | 0.004 | 991.631 | -0.001 |
| 055-L-SE-5-54 | 0.004 | 1110.489 | -0.004 |
| 061-L-SE-5-60 | 0.005 | 1229.357 | 0.000 |
| 067-L-SE-5-66 | 0.000 | 1348.232 | -0.003 |
| 073-L-SE-5-72 | 0.001 | 1467.106 | 0.004 |
| 079-L-SE-5-78 | 0.001 | 1585.970 | -0.001 |
| 085-L-SE-5-84 | 0.002 | 1704.837 | -0.001 |
| 091-L-SE-5-90 | -0.002 | 1823.721 | -0.001 |
| 095-L-SE-5-94 | -0.002 | 1902.953 | -0.001 |
| 007-L-SE-6-06 | 0.001 | 2131.553 | -0.001 |
| 011-L-SE-6-10 | 0.001 | 2210.794 | -0.001 |
| 017-L-SE-6-16 | -0.001 | 2329.668 | -0.001 |
| 023-L-SE-6-22 | -0.001 | 2448.524 | 0.005 |
| 029-L-SE-6-28 | 0.001 | 2567.407 | -0.002 |
| 035-L-SE-6-34 | -0.003 | 2686.290 | -0.001 |
| 041-L-SE-6-40 | -0.002 | 2805.137 | -0.004 |
| 047-L-SE-6-46 | -0.002 | 2924.026 | -0.001 |
| 053-L-SE-6-52 | 0.002 | 3042.895 | 0.000 |
| 059-L-SE-6-58 | -0.001 | 3161.757 | 0.001 |
| 065-L-SE-6-64 | 0.001 | 3280.631 | 0.002 |
| 071-L-SE-6-70 | -0.003 | 3399.507 | 0.001 |
| 077-L-SE-6-76 | -0.001 | 3518.382 | 0.002 |
| 083-L-SE-6-82 | -0.007 | 3637.281 | 0.000 |
| 089-L-SE-6-88 | -0.006 | 3756.135 | -0.002 |
| 095-L-SE-6-94 | -0.006 | 3875.00 | 0.003 |

The scatter of the residuals is presented graphically in **Figure 5** and **Figure 6**. **Figure 5** presents the scatter in the plane normal to the axis for each arm. There is an apparent greater right-left scatter along the X arm. This is a result means that the best description of the beam tube centerline positions corresponds to two axes which are not exactly orthogonal: an optimization without imposing the orthogonality constraint between the best fit lines results in axes having an included angle ~ 6.1 microradians greater than 90 degrees. This fact may be seen in the lower panels of **Figure 6** which present residuals in the horizontal and vertical plane as a function of their position along the arms.

Figure 5: Scatter plots of fit residuals in plane normal to global axis for Livingston, LA.

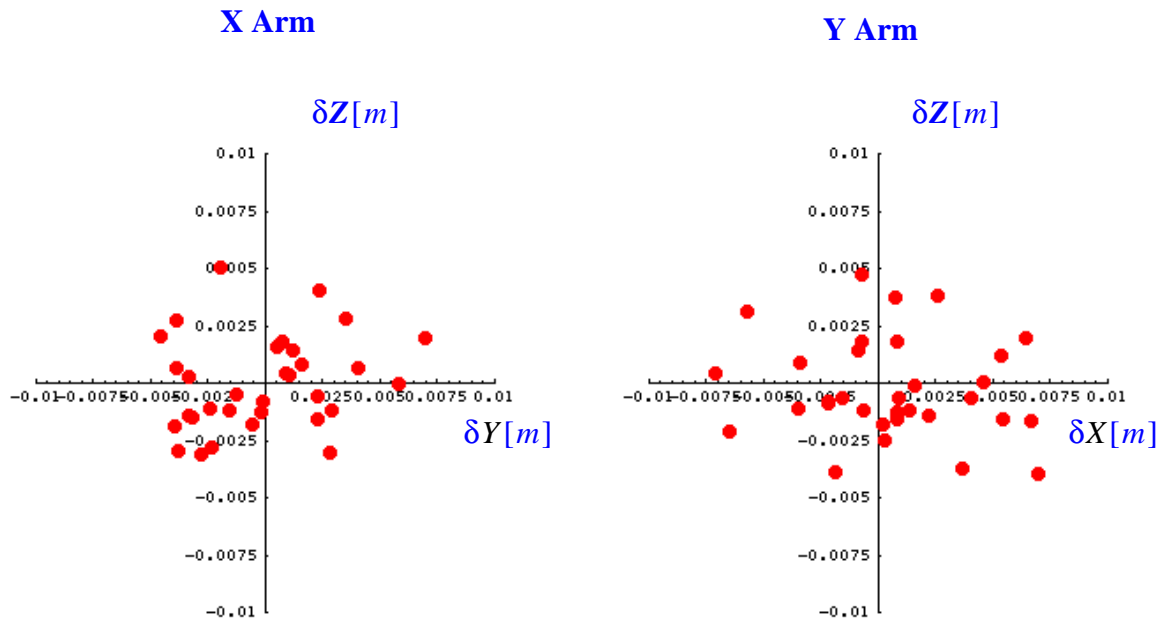
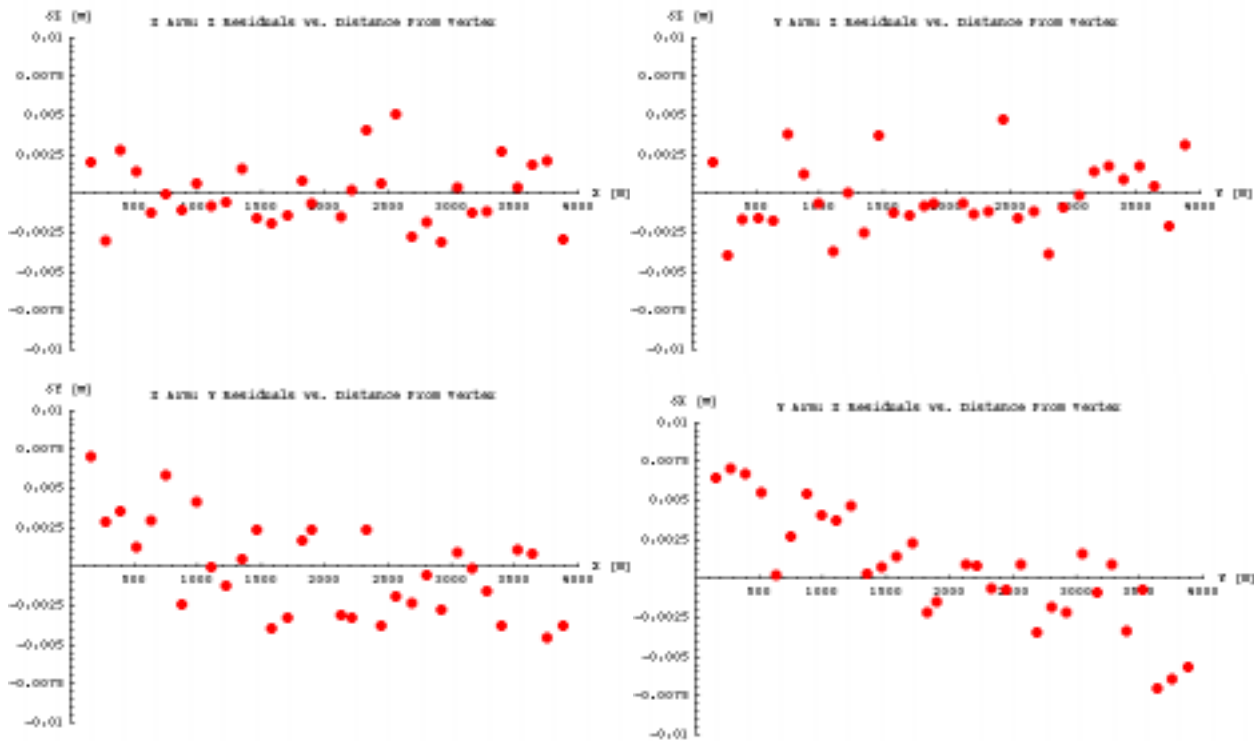


Figure 6: Dependence of residuals on distance along the arms for Livingston, LA.



3.2 Error propagators in the fits

Any error in the estimated position of the vertex results in a common mode offset to all marker positions; errors in the estimated directions of the coordinate axis result in either differential mode or common mode offsets according which orientation angle is in error and the effect on marker position is in proportion to marker distances from the vertex. This behavior is represented by the error propagation matrices presented as **Table 21**, **Table 22** and **Table 23**. Each table corresponds to one coordinate. The rows give the effects of parameter variations the eight marker locations. Vertex translational errors are referred along the global axes. Angular errors in the orientation of the axes are referred to roll, pitch and yaw of the \hat{z}_G axis. Refer to **Figure 4** in **Section 2.2** for definitions.

Table 21: Sensitivity matrix for the X_G coordinate for control points

| CB&I Marker ID | $\frac{\partial}{\partial V_x}$ [m/m] | $\frac{\partial}{\partial V_y}$ [m/m] | $\frac{\partial}{\partial V_z}$ [m/m] | $\frac{\partial}{\partial \theta_{CM}}$ [m/rad] | $\frac{\partial}{\partial \theta_{DM}}$ [m/rad] | $\frac{\partial}{\partial \theta_z}$ [m/rad] |
|----------------|------------------------------------------|------------------------------------------|------------------------------------------|----------------------------------------------------|----------------------------------------------------|-------------------------------------------------|
| X arm | | | | | | |
| 007-L-SW-7-06 | -0.955 | -0.142 | -0.262 | -0.001 | -0.001 | 0.007 |
| 013-L-SW-7-12 | -0.955 | -0.142 | -0.262 | 0.002 | 0.002 | 0.003 |
| 019-L-SW-7-18 | -0.955 | -0.142 | -0.262 | -0.002 | -0.002 | 0.004 |
| 025-L-SW-7-24 | -0.955 | -0.142 | -0.262 | -0.001 | -0.001 | 0.001 |
| 031-L-SW-7-30 | -0.955 | -0.142 | -0.262 | 0.001 | 0.001 | 0.003 |
| 037-L-SW-7-36 | -0.955 | -0.142 | -0.262 | 0.000 | 0.000 | 0.006 |
| 043-L-SW-7-42 | -0.955 | -0.142 | -0.262 | 0.001 | 0.001 | -0.002 |
| 049-L-SW-7-48 | -0.955 | -0.142 | -0.262 | 0.000 | 0.000 | 0.004 |
| 055-L-SW-7-54 | -0.955 | -0.142 | -0.262 | 0.001 | 0.001 | 0.000 |
| 061-L-SW-7-60 | -0.955 | -0.142 | -0.262 | 0.000 | 0.000 | -0.001 |
| 067-L-SW-7-66 | -0.955 | -0.142 | -0.262 | -0.001 | -0.001 | 0.001 |
| 073-L-SW-7-72 | -0.955 | -0.142 | -0.262 | 0.001 | 0.001 | 0.002 |
| 079-L-SW-7-78 | -0.955 | -0.142 | -0.262 | 0.001 | 0.001 | -0.004 |
| 085-L-SW-7-84 | -0.955 | -0.142 | -0.262 | 0.001 | 0.001 | -0.003 |
| 091-L-SW-7-90 | -0.955 | -0.142 | -0.262 | -0.001 | -0.001 | 0.002 |
| 095-L-SW-7-94 | -0.955 | -0.142 | -0.262 | 0.000 | 0.000 | 0.002 |
| 007-L-SW-8-06 | -0.955 | -0.142 | -0.262 | 0.001 | 0.001 | -0.003 |
| 011-L-SW-8-10 | -0.955 | -0.142 | -0.262 | 0.000 | 0.000 | -0.003 |
| 017-L-SW-8-16 | -0.955 | -0.142 | -0.262 | -0.003 | -0.003 | 0.002 |
| 023-L-SW-8-22 | -0.955 | -0.142 | -0.262 | 0.000 | 0.000 | -0.004 |
| 029-L-SW-8-28 | -0.955 | -0.142 | -0.262 | -0.004 | -0.004 | -0.002 |
| 035-L-SW-8-34 | -0.955 | -0.142 | -0.262 | 0.002 | 0.002 | -0.002 |
| 041-L-SW-8-40 | -0.955 | -0.142 | -0.262 | 0.001 | 0.001 | -0.001 |
| 047-L-SW-8-46 | -0.955 | -0.142 | -0.262 | 0.002 | 0.002 | -0.003 |
| 053-L-SW-8-52 | -0.955 | -0.142 | -0.262 | 0.000 | 0.000 | 0.001 |
| 059-L-SW-8-58 | -0.955 | -0.142 | -0.262 | 0.001 | 0.001 | 0.000 |
| 065-L-SW-8-64 | -0.955 | -0.142 | -0.262 | 0.001 | 0.001 | -0.002 |
| 071-L-SW-8-70 | -0.955 | -0.142 | -0.262 | -0.002 | -0.002 | -0.004 |
| 077-L-SW-8-76 | -0.955 | -0.142 | -0.262 | 0.000 | 0.000 | 0.001 |
| 083-L-SW-8-82 | -0.955 | -0.142 | -0.262 | -0.001 | -0.001 | 0.001 |
| 089-L-SW-8-88 | -0.955 | -0.142 | -0.262 | -0.001 | -0.001 | -0.005 |
| 095-L-SW-8-94 | -0.955 | -0.142 | -0.262 | 0.002 | 0.002 | -0.000 |

Table 21: Sensitivity matrix for the X_G coordinate for control points

| CB&I Marker ID | $\frac{\partial}{\partial V_x}$ [m/m] | $\frac{\partial}{\partial V_y}$ [m/m] | $\frac{\partial}{\partial V_z}$ [m/m] | $\frac{\partial}{\partial \theta_{CM}}$ [m/rad] | $\frac{\partial}{\partial \theta_{DM}}$ [m/rad] | $\frac{\partial}{\partial \theta_z}$ [m/rad] |
|----------------|------------------------------------------|------------------------------------------|------------------------------------------|----------------------------------------------------|----------------------------------------------------|-------------------------------------------------|
| Y arm | | | | | | |
| -L-SE-5-06 | -0.955 | -0.142 | -0.262 | -0.001 | -0.001 | 158.498 |
| 013-L-SE-5-12 | -0.955 | -0.142 | -0.262 | 0.003 | 0.003 | 278.366 |
| 019-L-SE-5-18 | -0.955 | -0.142 | -0.262 | 0.001 | 0.001 | 397.245 |
| 025-L-SE-5-24 | -0.955 | -0.142 | -0.262 | 0.001 | 0.001 | 516.135 |
| 031-L-SE-5-30 | -0.955 | -0.142 | -0.262 | 0.001 | 0.001 | 635.007 |
| 037-L-SE-5-36 | -0.955 | -0.142 | -0.262 | -0.003 | -0.003 | 753.883 |
| 043-L-SE-5-42 | -0.955 | -0.142 | -0.262 | -0.001 | -0.001 | 872.736 |
| 049-L-SE-5-48 | -0.955 | -0.142 | -0.262 | 0.000 | 0.000 | 991.631 |
| 055-L-SE-5-54 | -0.955 | -0.142 | -0.262 | 0.003 | 0.003 | 1110.489 |
| 061-L-SE-5-60 | -0.955 | -0.142 | -0.262 | 0.000 | 0.000 | 1229.357 |
| 067-L-SE-5-66 | -0.955 | -0.142 | -0.262 | 0.002 | 0.002 | 1348.232 |
| 073-L-SE-5-72 | -0.955 | -0.142 | -0.262 | -0.003 | -0.003 | 1467.106 |
| 079-L-SE-5-78 | -0.955 | -0.142 | -0.262 | 0.001 | 0.001 | 1585.97 |
| 085-L-SE-5-84 | -0.955 | -0.142 | -0.262 | 0.001 | 0.001 | 1704.837 |
| 091-L-SE-5-90 | -0.955 | -0.142 | -0.262 | 0.001 | 0.001 | 1823.721 |
| 095-L-SE-5-94 | -0.955 | -0.142 | -0.262 | 0.000 | 0.000 | 1902.953 |
| 007-L-SE-6-06 | -0.955 | -0.142 | -0.262 | 0.000 | 0.000 | 2131.553 |
| 011-L-SE-6-10 | -0.955 | -0.142 | -0.262 | 0.001 | 0.001 | 2210.794 |
| 017-L-SE-6-16 | -0.955 | -0.142 | -0.262 | 0.001 | 0.001 | 2329.668 |
| 023-L-SE-6-22 | -0.955 | -0.142 | -0.262 | -0.003 | -0.003 | 2448.524 |
| 029-L-SE-6-28 | -0.955 | -0.142 | -0.262 | 0.001 | 0.001 | 2567.407 |
| 035-L-SE-6-34 | -0.955 | -0.142 | -0.262 | 0.001 | 0.001 | 2686.29 |
| 041-L-SE-6-40 | -0.955 | -0.142 | -0.262 | 0.003 | 0.003 | 2805.137 |
| 047-L-SE-6-46 | -0.955 | -0.142 | -0.262 | 0.001 | 0.001 | 2924.026 |
| 053-L-SE-6-52 | -0.955 | -0.142 | -0.262 | 0.000 | 0.000 | 3042.895 |
| 059-L-SE-6-58 | -0.955 | -0.142 | -0.262 | -0.001 | -0.001 | 3161.757 |
| 065-L-SE-6-64 | -0.955 | -0.142 | -0.262 | -0.001 | -0.001 | 3280.631 |
| 071-L-SE-6-70 | -0.955 | -0.142 | -0.262 | -0.001 | -0.001 | 3399.507 |
| 077-L-SE-6-76 | -0.955 | -0.142 | -0.262 | -0.001 | -0.001 | 3518.382 |
| 083-L-SE-6-82 | -0.955 | -0.142 | -0.262 | 0.000 | 0.000 | 3637.281 |
| 089-L-SE-6-88 | -0.955 | -0.142 | -0.262 | 0.001 | 0.001 | 3756.135 |
| 095-L-SE-6-94 | -0.955 | -0.142 | -0.262 | -0.002 | -0.002 | 3875.008 |

Table 22: Sensitivity matrix for the Y_G coordinate for control points

| CB&I Marker ID | $\frac{\partial}{\partial V_x}$ [m/m] | $\frac{\partial}{\partial V_y}$ [m/m] | $\frac{\partial}{\partial V_z}$ [m/m] | $\frac{\partial}{\partial \theta_{CM}}$ [m/rad] | $\frac{\partial}{\partial \theta_{DM}}$ [m/rad] | $\frac{\partial}{\partial \theta_z}$ [m/rad] |
|----------------|------------------------------------------|------------------------------------------|------------------------------------------|----------------------------------------------------|----------------------------------------------------|-------------------------------------------------|
| X arm | | | | | | |
| 007-L-SW-7-06 | 0.298 | -0.488 | -0.821 | -0.001 | 0.001 | -159.498 |
| 013-L-SW-7-12 | 0.298 | -0.488 | -0.821 | 0.002 | -0.002 | -278.385 |
| 019-L-SW-7-18 | 0.298 | -0.488 | -0.821 | -0.002 | 0.002 | -397.252 |
| 025-L-SW-7-24 | 0.298 | -0.488 | -0.821 | -0.001 | 0.001 | -516.133 |
| 031-L-SW-7-30 | 0.298 | -0.488 | -0.821 | 0.001 | -0.001 | -634.996 |
| 037-L-SW-7-36 | 0.298 | -0.488 | -0.821 | 0.000 | 0.000 | -753.868 |
| 043-L-SW-7-42 | 0.298 | -0.488 | -0.821 | 0.001 | -0.001 | -872.738 |
| 049-L-SW-7-48 | 0.298 | -0.488 | -0.821 | 0.000 | 0.000 | -991.613 |
| 055-L-SW-7-54 | 0.298 | -0.488 | -0.821 | 0.001 | -0.001 | -1110.485 |
| 061-L-SW-7-60 | 0.298 | -0.488 | -0.821 | 0.000 | 0.000 | -1229.356 |
| 067-L-SW-7-66 | 0.298 | -0.488 | -0.821 | -0.001 | 0.001 | -1348.235 |
| 073-L-SW-7-72 | 0.298 | -0.488 | -0.821 | 0.001 | -0.001 | -1467.1 |
| 079-L-SW-7-78 | 0.298 | -0.488 | -0.821 | 0.001 | -0.001 | -1585.967 |
| 085-L-SW-7-84 | 0.298 | -0.488 | -0.821 | 0.001 | -0.001 | -1704.837 |
| 091-L-SW-7-90 | 0.298 | -0.488 | -0.821 | -0.001 | 0.001 | -1823.743 |
| 095-L-SW-7-94 | 0.298 | -0.488 | -0.821 | 0.000 | 0.000 | -1902.992 |
| 007-L-SW-8-06 | 0.298 | -0.488 | -0.821 | 0.001 | -0.001 | -2131.541 |
| 011-L-SW-8-10 | 0.298 | -0.488 | -0.821 | 0.000 | 0.000 | -2210.78 |
| 017-L-SW-8-16 | 0.298 | -0.488 | -0.821 | -0.003 | 0.003 | -2329.661 |
| 023-L-SW-8-22 | 0.298 | -0.488 | -0.821 | 0.000 | 0.000 | -2448.533 |
| 029-L-SW-8-28 | 0.298 | -0.488 | -0.821 | -0.004 | 0.004 | -2567.4 |
| 035-L-SW-8-34 | 0.298 | -0.488 | -0.821 | 0.002 | -0.002 | -2686.268 |
| 041-L-SW-8-40 | 0.298 | -0.488 | -0.821 | 0.001 | -0.001 | -2805.145 |
| 047-L-SW-8-46 | 0.298 | -0.488 | -0.821 | 0.002 | -0.002 | -2924.016 |
| 053-L-SW-8-52 | 0.298 | -0.488 | -0.821 | 0.000 | 0.000 | -3042.891 |
| 059-L-SW-8-58 | 0.298 | -0.488 | -0.821 | 0.001 | -0.001 | -3161.765 |
| 065-L-SW-8-64 | 0.298 | -0.488 | -0.821 | 0.001 | -0.001 | -3280.63 |
| 071-L-SW-8-70 | 0.298 | -0.488 | -0.821 | -0.002 | 0.002 | -3399.494 |
| 077-L-SW-8-76 | 0.298 | -0.488 | -0.821 | 0.000 | 0.000 | -3518.365 |
| 083-L-SW-8-82 | 0.298 | -0.488 | -0.821 | -0.001 | 0.001 | -3637.242 |
| 089-L-SW-8-88 | 0.298 | -0.488 | -0.821 | -0.001 | 0.001 | -3756.121 |
| 095-L-SW-8-94 | 0.298 | -0.488 | -0.821 | 0.002 | -0.002 | -3875.009 |

Table 22: Sensitivity matrix for the Y_G coordinate for control points

| CB&I Marker ID | $\frac{\partial}{\partial V_x}$ [m/m] | $\frac{\partial}{\partial V_y}$ [m/m] | $\frac{\partial}{\partial V_z}$ [m/m] | $\frac{\partial}{\partial \theta_{CM}}$ [m/rad] | $\frac{\partial}{\partial \theta_{DM}}$ [m/rad] | $\frac{\partial}{\partial \theta_z}$ [m/rad] |
|----------------|------------------------------------------|------------------------------------------|------------------------------------------|----------------------------------------------------|----------------------------------------------------|-------------------------------------------------|
| Y arm | | | | | | |
| -L-SE-5-06 | 0.298 | -0.488 | -0.821 | -0.001 | 0.001 | -0.006 |
| 013-L-SE-5-12 | 0.298 | -0.488 | -0.821 | 0.003 | -0.003 | -0.007 |
| 019-L-SE-5-18 | 0.298 | -0.488 | -0.821 | 0.001 | -0.001 | -0.007 |
| 025-L-SE-5-24 | 0.298 | -0.488 | -0.821 | 0.001 | -0.001 | -0.005 |
| 031-L-SE-5-30 | 0.298 | -0.488 | -0.821 | 0.001 | -0.001 | 0.000 |
| 037-L-SE-5-36 | 0.298 | -0.488 | -0.821 | -0.003 | 0.003 | -0.003 |
| 043-L-SE-5-42 | 0.298 | -0.488 | -0.821 | -0.001 | 0.001 | -0.005 |
| 049-L-SE-5-48 | 0.298 | -0.488 | -0.821 | 0.000 | 0.000 | -0.004 |
| 055-L-SE-5-54 | 0.298 | -0.488 | -0.821 | 0.003 | -0.003 | -0.004 |
| 061-L-SE-5-60 | 0.298 | -0.488 | -0.821 | 0.000 | 0.000 | -0.005 |
| 067-L-SE-5-66 | 0.298 | -0.488 | -0.821 | 0.002 | -0.002 | 0.000 |
| 073-L-SE-5-72 | 0.298 | -0.488 | -0.821 | -0.003 | 0.003 | -0.001 |
| 079-L-SE-5-78 | 0.298 | -0.488 | -0.821 | 0.001 | -0.001 | -0.001 |
| 085-L-SE-5-84 | 0.298 | -0.488 | -0.821 | 0.001 | -0.001 | -0.002 |
| 091-L-SE-5-90 | 0.298 | -0.488 | -0.821 | 0.001 | -0.001 | 0.002 |
| 095-L-SE-5-94 | 0.298 | -0.488 | -0.821 | 0.000 | 0.000 | 0.002 |
| 007-L-SE-6-06 | 0.298 | -0.488 | -0.821 | 0.000 | 0.000 | -0.001 |
| 011-L-SE-6-10 | 0.298 | -0.488 | -0.821 | 0.001 | -0.001 | -0.001 |
| 017-L-SE-6-16 | 0.298 | -0.488 | -0.821 | 0.001 | -0.001 | 0.001 |
| 023-L-SE-6-22 | 0.298 | -0.488 | -0.821 | -0.003 | 0.003 | 0.001 |
| 029-L-SE-6-28 | 0.298 | -0.488 | -0.821 | 0.001 | -0.001 | -0.001 |
| 035-L-SE-6-34 | 0.298 | -0.488 | -0.821 | 0.001 | -0.001 | 0.003 |
| 041-L-SE-6-40 | 0.298 | -0.488 | -0.821 | 0.003 | -0.003 | 0.002 |
| 047-L-SE-6-46 | 0.298 | -0.488 | -0.821 | 0.001 | -0.001 | 0.002 |
| 053-L-SE-6-52 | 0.298 | -0.488 | -0.821 | 0.000 | 0.000 | -0.002 |
| 059-L-SE-6-58 | 0.298 | -0.488 | -0.821 | -0.001 | 0.001 | 0.001 |
| 065-L-SE-6-64 | 0.298 | -0.488 | -0.821 | -0.001 | 0.001 | -0.001 |
| 071-L-SE-6-70 | 0.298 | -0.488 | -0.821 | -0.001 | 0.001 | 0.003 |
| 077-L-SE-6-76 | 0.298 | -0.488 | -0.821 | -0.001 | 0.001 | 0.001 |
| 083-L-SE-6-82 | 0.298 | -0.488 | -0.821 | 0.000 | 0.000 | 0.007 |
| 089-L-SE-6-88 | 0.298 | -0.488 | -0.821 | 0.001 | -0.001 | 0.006 |
| 095-L-SE-6-94 | 0.298 | -0.488 | -0.821 | -0.002 | 0.002 | 0.006 |

Table 23: Sensitivity matrix for the Z_G coordinate for control points

| CB&I Marker ID | $\frac{\partial}{\partial V_x}$ [m/m] | $\frac{\partial}{\partial V_y}$ [m/m] | $\frac{\partial}{\partial V_z}$ [m/m] | $\frac{\partial}{\partial \theta_{CM}}$ [m/rad] | $\frac{\partial}{\partial \theta_{DM}}$ [m/rad] | $\frac{\partial}{\partial \theta_z}$ [m/rad] |
|----------------|------------------------------------------|------------------------------------------|------------------------------------------|----------------------------------------------------|----------------------------------------------------|-------------------------------------------------|
| X arm | | | | | | |
| 007-L-SW-7-06 | -0.012 | -0.861 | 0.508 | 112.787 | 112.777 | 0 |
| 013-L-SW-7-12 | -0.012 | -0.861 | 0.508 | 196.85 | 196.846 | 0 |
| 019-L-SW-7-18 | -0.012 | -0.861 | 0.508 | 280.902 | 280.897 | 0 |
| 025-L-SW-7-24 | -0.012 | -0.861 | 0.508 | 364.962 | 364.96 | 0 |
| 031-L-SW-7-30 | -0.012 | -0.861 | 0.508 | 449.012 | 449.008 | 0 |
| 037-L-SW-7-36 | -0.012 | -0.861 | 0.508 | 533.069 | 533.061 | 0 |
| 043-L-SW-7-42 | -0.012 | -0.861 | 0.508 | 617.117 | 617.121 | 0 |
| 049-L-SW-7-48 | -0.012 | -0.861 | 0.508 | 701.179 | 701.173 | 0 |
| 055-L-SW-7-54 | -0.012 | -0.861 | 0.508 | 785.231 | 785.231 | 0 |
| 061-L-SW-7-60 | -0.012 | -0.861 | 0.508 | 869.285 | 869.287 | 0 |
| 067-L-SW-7-66 | -0.012 | -0.861 | 0.508 | 953.346 | 953.346 | 0 |
| 073-L-SW-7-72 | -0.012 | -0.861 | 0.508 | 1037.398 | 1037.394 | 0 |
| 079-L-SW-7-78 | -0.012 | -0.861 | 0.508 | 1121.446 | 1121.451 | 0 |
| 085-L-SW-7-84 | -0.012 | -0.861 | 0.508 | 1205.5 | 1205.504 | 0 |
| 091-L-SW-7-90 | -0.012 | -0.861 | 0.508 | 1289.582 | 1289.58 | 0 |
| 095-L-SW-7-94 | -0.012 | -0.861 | 0.508 | 1345.62 | 1345.617 | 0 |
| 007-L-SW-8-06 | -0.012 | -0.861 | 0.508 | 1507.225 | 1507.229 | 0 |
| 011-L-SW-8-10 | -0.012 | -0.861 | 0.508 | 1563.255 | 1563.26 | 0 |
| 017-L-SW-8-16 | -0.012 | -0.861 | 0.508 | 1647.321 | 1647.317 | 0 |
| 023-L-SW-8-22 | -0.012 | -0.861 | 0.508 | 1731.371 | 1731.377 | 0 |
| 029-L-SW-8-28 | -0.012 | -0.861 | 0.508 | 1815.425 | 1815.428 | 0 |
| 035-L-SW-8-34 | -0.012 | -0.861 | 0.508 | 1899.477 | 1899.48 | 0 |
| 041-L-SW-8-40 | -0.012 | -0.861 | 0.508 | 1983.537 | 1983.538 | 0 |
| 047-L-SW-8-46 | -0.012 | -0.861 | 0.508 | 2067.59 | 2067.594 | 0 |
| 053-L-SW-8-52 | -0.012 | -0.861 | 0.508 | 2151.65 | 2151.648 | 0 |
| 059-L-SW-8-58 | -0.012 | -0.861 | 0.508 | 2235.705 | 2235.705 | 0 |
| 065-L-SW-8-64 | -0.012 | -0.861 | 0.508 | 2319.754 | 2319.757 | 0 |
| 071-L-SW-8-70 | -0.012 | -0.861 | 0.508 | 2403.802 | 2403.808 | 0 |
| 077-L-SW-8-76 | -0.012 | -0.861 | 0.508 | 2487.861 | 2487.859 | 0 |
| 083-L-SW-8-82 | -0.012 | -0.861 | 0.508 | 2571.919 | 2571.918 | 0 |
| 089-L-SW-8-88 | -0.012 | -0.861 | 0.508 | 2655.976 | 2655.982 | 0 |
| 095-L-SW-8-94 | -0.012 | -0.861 | 0.508 | 2740.043 | 2740.048 | 0 |

Table 23: Sensitivity matrix for the Z_G coordinate for control points

| CB&I Marker ID | $\frac{\partial}{\partial V_x}$ [m/m] | $\frac{\partial}{\partial V_y}$ [m/m] | $\frac{\partial}{\partial V_z}$ [m/m] | $\frac{\partial}{\partial \theta_{CM}}$ [m/rad] | $\frac{\partial}{\partial \theta_{DM}}$ [m/rad] | $\frac{\partial}{\partial \theta_z}$ [m/rad] |
|----------------|------------------------------------------|------------------------------------------|------------------------------------------|----------------------------------------------------|----------------------------------------------------|-------------------------------------------------|
| Y arm | | | | | | |
| -L-SE-5-06 | -0.012 | -0.861 | 0.508 | 112.08 | -112.071 | 0 |
| 013-L-SE-5-12 | -0.012 | -0.861 | 0.508 | 196.84 | -196.83 | 0 |
| 019-L-SE-5-18 | -0.012 | -0.861 | 0.508 | 280.9 | -280.89 | 0 |
| 025-L-SE-5-24 | -0.012 | -0.861 | 0.508 | 364.967 | -364.959 | 0 |
| 031-L-SE-5-30 | -0.012 | -0.861 | 0.508 | 449.018 | -449.018 | 0 |
| 037-L-SE-5-36 | -0.012 | -0.861 | 0.508 | 533.078 | -533.074 | 0 |
| 043-L-SE-5-42 | -0.012 | -0.861 | 0.508 | 617.121 | -617.114 | 0 |
| 049-L-SE-5-48 | -0.012 | -0.861 | 0.508 | 701.192 | -701.186 | 0 |
| 055-L-SE-5-54 | -0.012 | -0.861 | 0.508 | 785.237 | -785.232 | 0 |
| 061-L-SE-5-60 | -0.012 | -0.861 | 0.508 | 869.29 | -869.283 | 0 |
| 067-L-SE-5-66 | -0.012 | -0.861 | 0.508 | 953.344 | -953.344 | 0 |
| 073-L-SE-5-72 | -0.012 | -0.861 | 0.508 | 1037.401 | -1037.4 | 0 |
| 079-L-SE-5-78 | -0.012 | -0.861 | 0.508 | 1121.451 | -1121.449 | 0 |
| 085-L-SE-5-84 | -0.012 | -0.861 | 0.508 | 1205.504 | -1205.5 | 0 |
| 091-L-SE-5-90 | -0.012 | -0.861 | 0.508 | 1289.564 | -1289.567 | 0 |
| 095-L-SE-5-94 | -0.012 | -0.861 | 0.508 | 1345.59 | -1345.592 | 0 |
| 007-L-SE-6-06 | -0.012 | -0.861 | 0.508 | 1507.236 | -1507.235 | 0 |
| 011-L-SE-6-10 | -0.012 | -0.861 | 0.508 | 1563.268 | -1563.267 | 0 |
| 017-L-SE-6-16 | -0.012 | -0.861 | 0.508 | 1647.323 | -1647.324 | 0 |
| 023-L-SE-6-22 | -0.012 | -0.861 | 0.508 | 1731.367 | -1731.368 | 0 |
| 029-L-SE-6-28 | -0.012 | -0.861 | 0.508 | 1815.431 | -1815.43 | 0 |
| 035-L-SE-6-34 | -0.012 | -0.861 | 0.508 | 1899.492 | -1899.497 | 0 |
| 041-L-SE-6-40 | -0.012 | -0.861 | 0.508 | 1983.53 | -1983.533 | 0 |
| 047-L-SE-6-46 | -0.012 | -0.861 | 0.508 | 2067.597 | -2067.6 | 0 |
| 053-L-SE-6-52 | -0.012 | -0.861 | 0.508 | 2151.653 | -2151.651 | 0 |
| 059-L-SE-6-58 | -0.012 | -0.861 | 0.508 | 2235.699 | -2235.7 | 0 |
| 065-L-SE-6-64 | -0.012 | -0.861 | 0.508 | 2319.757 | -2319.756 | 0 |
| 071-L-SE-6-70 | -0.012 | -0.861 | 0.508 | 2403.812 | -2403.817 | 0 |
| 077-L-SE-6-76 | -0.012 | -0.861 | 0.508 | 2487.871 | -2487.872 | 0 |
| 083-L-SE-6-82 | -0.012 | -0.861 | 0.508 | 2571.941 | -2571.951 | 0 |
| 089-L-SE-6-88 | -0.012 | -0.861 | 0.508 | 2655.984 | -2655.993 | 0 |
| 095-L-SE-6-94 | -0.012 | -0.861 | 0.508 | 2740.040 | -2740.048 | 0 |

Table 24 presents uncertainties in vertex position and axis orientations. The uncertainties were defined as the amount of parameter variation which results in a doubling of the RMS residuals from the minimum value 0.0042 m. The vector in **Table 24** may be multiplied by each of the previous tables to obtain the (correlated) errors in marker positions.

Table 24: Uncertainties in fitted parameters. Changing the best fit values by these amounts result in a doubling of the RMS residual fitting error.

| Parameter | Error |
|---------------|--------------------------|
| V_x | 0.0062 m |
| V_x | 0.0055 m |
| V_x | 0.0038 m |
| θ_{CM} | $2.44 \cdot 10^{-6}$ rad |
| θ_{DM} | $2.44 \cdot 10^{-6}$ rad |
| θ_z | $1.72 \cdot 10^{-6}$ rad |

3.3 Livingston Local Coordinate Systems in each station

Table 25, **Table 26** and **Table 27** present the direction cosines between the global coordinate system and the local coordinate systems for each station. The local coordinates are defined in LIGO-L950128 and LIGO-T950004 listed in **Table 1**.

Table 25: Livingston Vertex Global-Local System Direction Cosines

| | \hat{x}_L | \hat{y}_L | \hat{z}_L |
|-------------|---------------------------|---------------------------|---------------------------|
| \hat{x}_G | $1 - 4.872 \cdot 10^{-8}$ | 0 | -0.000312 |
| \hat{y}_G | $-1.90619 \cdot 10^{-7}$ | $1 - 1.865 \cdot 10^{-7}$ | -0.0006107 |
| \hat{z}_G | 0.000312 | 0.0006107 | $1 - 2.352 \cdot 10^{-7}$ |

Table 26: Livingston X End Station (d= 4000m) Global-Local System Direction Cosines

| | \hat{x}_L | \hat{y}_L | \hat{z}_L |
|-------------|---------------------------|---------------------------|---------------------------|
| \hat{x}_G | $1 - 4.953 \cdot 10^{-8}$ | 0 | 0.0003147 |
| \hat{y}_G | $1.919 \cdot 10^{-7}$ | $1 - 1.859 \cdot 10^{-7}$ | -0.00060980 |
| \hat{z}_G | -0.0003147 | 0.0006098 | $1 - 2.354 \cdot 10^{-7}$ |

Table 27: Livingston Y End Station (d= 4000m) Global-Local System Direction Cosines

| | \hat{x}_L | \hat{y}_L | \hat{z}_L |
|-------------|---------------------------|----------------------------|---------------------------|
| \hat{x}_G | $1 - 4.843 \cdot 10^{-8}$ | 0 | -0.0003112 |
| \hat{y}_G | $5.840 \cdot 10^{-9}$ | $1 - 1.761 \cdot 10^{-10}$ | 0.00001877 |
| \hat{z}_G | 0.0003112 | -0.00001877 | $1 - 4.861 \cdot 10^{-8}$ |

3.4 Positions of LIGO Primary GPS Monuments in the Global Coordinate System

The Livingston site has surveyed array of 19 primary GPS monuments. The data in **Table 28** present the SJB survey results as report on an SJB drawing, signed and dated 19 September 1997.

Table 28: Report Geodetic Coordinates for the GPS primary monuments at Livingston^a

| Monument ID | <i>Latitude[N]</i> | | | <i>Longitude[W]</i> | | | <i>Ellipsoidal height of marker</i> |
|--------------------|--------------------|----|-----------|---------------------|----|------------|-------------------------------------|
| | ° | ' | " | ° | ' | " | <i>m</i> |
| LIGO 1 | 30 | 31 | 47.14036 | 90 | 45 | 42.28956 | -11.6910 |
| LIGO 2 | 30 | 32 | 45.77207 | 90 | 46 | 3.605033 | -10.4008 |
| LIGO 3 | 30 | 33 | 45.57113 | 90 | 46 | 23.895763 | -8.3971 |
| LIGO 4 | 30 | 33 | 28.144005 | 90 | 47 | 37.33406 | -8.3762 |
| LIGO 5 | 30 | 33 | 9.222812 | 90 | 48 | 50.44142 | -9.2898 |
| LIGO 101 | 30 | 33 | 9.138402 | 90 | 48 | 46.04203 | -8.8302 |
| LIGO 103 | 30 | 33 | 14.283633 | 90 | 48 | 27.463132 | -8.8923 |
| LIGO 105 | 30 | 33 | 19.111329 | 90 | 48 | 10.039553 | -9.8332 |
| LIGO 107 | 30 | 33 | 23.632935 | 90 | 47 | 53.64897 | -8.5603 |
| LIGO 111 | 30 | 33 | 33.27441 | 90 | 47 | 18.825012 | -8.9727 |
| LIGO 113 | 30 | 33 | 38.39051 | 90 | 47 | 0.30096100 | -9.4351 |
| LIGO 115 | 30 | 33 | 44.88060 | 90 | 46 | 35.10847 | -9.6865 |
| LIGO 114 | 30 | 33 | 41.98956 | 90 | 46 | 24.553803 | -9.2624 |

Table 28: Report Geodetic Coordinates for the GPS primary monuments at Livingston^a

| <i>Monument ID</i> | <i>Latitude[N]</i> | | | <i>Longitude[W]</i> | | | <i>Ellipsoidal height of marker</i> |
|--------------------|--------------------|----|-----------|---------------------|----|-----------|-------------------------------------|
| | ° | ' | " | ° | ' | " | <i>m</i> |
| LIGO 112 | 30 | 33 | 30.714303 | 90 | 46 | 20.319260 | -9.5362 |
| LIGO 110 | 30 | 33 | 13.701668 | 90 | 46 | 14.055644 | -9.7217 |
| LIGO 108 | 30 | 33 | 0.4880430 | 90 | 46 | 9.226404 | -10.2545 |
| LIGO 106 | 30 | 32 | 29.385051 | 90 | 45 | 57.76082 | -11.5090 |
| LIGO 104 | 30 | 32 | 13.320793 | 90 | 45 | 51.86420 | -11.5959 |
| LIGO 102 | 30 | 31 | 59.20009 | 90 | 45 | 46.66725 | -11.6330 |

a. SJB provided orthometric heights only; the height of the geoid relative to the WGS84 ellipsoid was calculated using the GEOID96 FORTRAN program available from the US Geodetic Survey.

Figure 7: Layout of the CB&I control points and primary GPS monument array at Livingston. Dots (colored) denote the CB&I control points for alignment of the beam tubes; plus signs denote the primary GPS monuments.

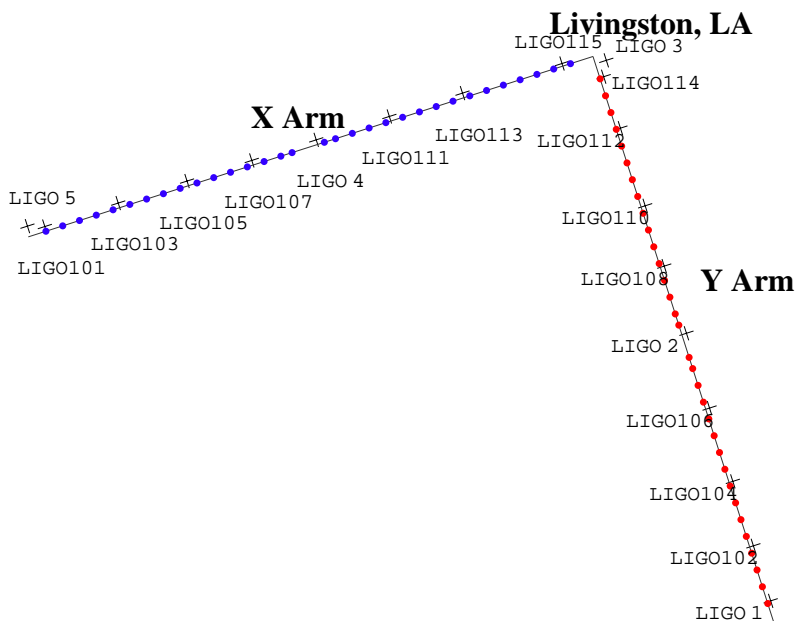


Figure 7 depicts graphically the overall site layout, including CB&I control points, beam tube centerlines and primary GPS monuments.

Table 29 presents the calculated locations of the primary GPS monuments in the site global coor-

dinate system. Dimensions are in meters.

Table 29: Position of the GPS primary monuments in the site global coordinate system

| Monument ID | X_G | Y_G | Z_G |
|-------------|------------|------------|------------|
| LIGO 1 | -24.354011 | 3863.778 | -3.940493 |
| LIGO 2 | -32.39879 | 1970.9518 | -2.9398506 |
| LIGO 3 | -77.58747 | 52.21562 | -1.8169736 |
| LIGO 4 | 1950.0210 | -32.30165 | -1.5120938 |
| LIGO 5 | 3983.322 | -70.70532 | -2.7601553 |
| LIGO 101 | 3872.435 | -32.51023 | -2.2432689 |
| LIGO 103 | 3352.541 | -32.59589 | -2.1733581 |
| LIGO 105 | 2864.9596 | -32.77025 | -3.0290268 |
| LIGO 107 | 2406.4779 | -32.37370 | -1.7095796 |
| LIGO 111 | 1432.0647 | -32.61503 | -2.1331897 |
| LIGO 113 | 913.8685 | -32.41294 | -2.6619423 |
| LIGO 115 | 213.52234 | -18.458987 | -3.0615683 |
| LIGO 114 | -27.319999 | 151.94342 | -2.6068115 |
| LIGO 112 | -29.160738 | 517.0383 | -2.6774962 |
| LIGO 110 | -28.761831 | 1066.8928 | -2.5956056 |
| LIGO 108 | -27.557296 | 1493.6743 | -2.9534150 |
| LIGO 106 | -27.254956 | 2499.0584 | -3.909666 |
| LIGO 104 | -26.480611 | 3018.1235 | -3.904589 |
| LIGO 102 | -26.160749 | 3474.502 | -3.896069 |

4 GRAPHICAL REPRESENTATIONS OF THE INTERFEROMETER PLANES FOR EACH SITE

Figure 8 presents graphical representations of the orientations of the interferometer planes at the two sites relative to a surface of constant elevation (referred to the vertex) from various points of view. A spherical earth was assumed in generating the pictures (deviations from geoid or ellipsoid do not affect results at the level of precision required).

Figure 8: Representation of the interferometer plane inclinations at the two LIGO sites.

